

# Kinematic and Spatial Substructure in NGC 2264<sup>1</sup>

John J. Tobin<sup>2,5</sup>, Lee Hartmann<sup>3</sup>, Gabor Fűrész<sup>4</sup>, Wen-Hsin Hsu<sup>3</sup>, Mario Mateo<sup>3</sup>

## ABSTRACT

We present an expanded kinematic study of the young cluster NGC 2264 based upon optical radial velocities measured using multi-fiber echelle spectroscopy at the 6.5 meter MMT and Magellan telescopes. We report radial velocities for 695 stars, of which approximately 407 stars are confirmed or very likely members. Our results more than double the number of members with radial velocities from Fűrész *et al.*, resulting in a much better defined kinematic relationship between the stellar population and the associated molecular gas. In particular, we find that there is a significant subset of stars that are systematically blueshifted with respect to the molecular (<sup>13</sup>CO) gas. The detection of Lithium absorption and/or infrared excesses in this blue-shifted population suggests that at least some of these stars are cluster members; we suggest some speculative scenarios to explain their kinematics. Our results also more clearly define the redshifted population of stars in the northern end of the cluster; we suggest that the stellar and gas kinematics of this region are the result of a bubble driven by the wind from O7 star S Mon. Our results emphasize the complexity of the spatial and kinematic structure of NGC 2264, important for eventually building up a comprehensive picture of cluster formation.

*Subject headings:* stars: formation

## 1. Introduction

Most stars form in clusters (Carpenter 2000; Lada & Lada 2003; Allen et al. 2007; Krumholz et al. 2014), and it is important to understand the processes that lead to the formation of these clusters, in addition to physics of the formation of the individual stars themselves. Star cluster formation

---

<sup>1</sup>Observations reported here were obtained at the MMT Observatory, a joint facility of the Smithsonian Institution and the University of Arizona; This paper includes data gathered with the 6.5 meter Magellan Telescopes located at Las Campanas Observatory, Chile

<sup>2</sup>Hubble Fellow, National Radio Astronomy Observatory, Charlottesville, VA 22903

<sup>3</sup>Department of Astronomy, University of Michigan, Ann Arbor, MI 48109

<sup>4</sup>Center for Astrophysics, 60 Garden Street, Cambridge, MA 02138

<sup>5</sup>Current Address: Leiden Observatory, Leiden University, P.O. Box 9513, 2300-RA Leiden, The Netherlands; tobin@strw.leidenuniv.nl

theories are generally comprised of two classes: highly dynamic, non-equilibrium models that form within a crossing time (e.g. Bonnell et al. 2003; Bate 2012) and quasi-equilibrium and/or slow contraction scenarios that require several crossing times to form (e.g., Tan et al. 2006). Studies of both the spatial distribution of stars (e.g., Feigelson et al. 2013) and their kinematics (e.g., Fűrész et al. 2006, 2008; Tobin et al. 2009; Cottaar et al. 2014; Foster et al. 2014) in young clusters that may not be dynamically relaxed and still have substantial mass in molecular gas can help distinguish between these two main possibilities.

The closest region of significant clustered star formation after the Orion Nebula Cluster is NGC 2264 (see Dahm 2008) at a distance of  $\sim 760 - 900$  pc (Sung et al. 1997; Baxter et al. 2009). This cluster is spatially elongated along a distance  $\sim 8$  pc with significant sub-clusterings. Combining mid-infrared data from the *Spitzer Space Telescope* with previous optical photometric and  $H\alpha$  emission surveys, Sung et al. (2009) identified several distinct regions: a large, extended region of low extinction  $\sim 3.5$  pc in diameter centered on the O7V + B1.5V binary S Mon (Skiff 2013). The two other sub-clusters are the “Cone” and “Spokes” (Texeira et al. 2006), and they are denser and more highly extinguished, each centered around very luminous protostars. Sung et al. (2008) and Feigelson et al. (2013) also highlighted a “halo” population of young stars that were distributed throughout the cluster.

Fűrész et al. (2006) (Paper I) found a strong correlation between the velocities of the molecular gas and the associated stellar population as a function of position, with the optically-visible members of the subclusters showing distinct velocity components. The correlation of spatial substructure with kinematics clearly demonstrates that NGC 2264 is not dynamically relaxed, consistent with the youth of the stellar population (Sung et al. 2008, 2009). In this paper we present new radial velocity observations which, when added to the previous measurements over the past six years, enable a refined study of the spatio-kinematic structure of the cluster. We defer a characterization of the spectroscopic binary population to a subsequent paper. While the overall correlation between stellar and gas motions remains much the same as in Fűrész et al. (2006), we find additional velocity substructure that was not apparent in our initial study. The results contribute to the development of a quantitative picture of the kinematics of NGC 2264 which can ultimately be used as a testing ground for theories of cluster formation.

## 2. Observations and Data Reduction

### 2.1. Target Selection

Because of the proximity of NGC 2264 to the Galactic Plane, careful selection of candidate members was necessary to reduce contamination as much as possible. This continuing study uses the same target selection from Fűrész et al. (2006) which drew sources from X-ray (Ramírez et al. 2004),  $H\alpha$  surveys, and some additional sources showing UV or IR excess from Park et al. (2000). We have added additional targets from Rebull et al. (2002) whose V-band magnitudes fall within

the range of magnitudes expected for cluster members. Selection from these catalogs attempts to identify pre-main sequence cluster members in different stages of evolution; stars from the  $H\alpha$  and Park et al. (2000) optical study will preferentially find Classical T Tauri Stars (CTTSs) or Class II accreting objects while the X-ray sources will find Class III or weak T Tauri Stars (WTTSs) without substantial accretion activity. The additional targets from Rebull et al. (2002) are meant to fill unused fibers, enabling us to identify additional members not selected based on other criteria.

A subset of stars whose membership was questionable because their radial velocities differ significantly from the molecular gas in the region (the “blueshifted population”; section 3 and 4.2) were selected as the main targets for multi-slit observations with the Inamori-Magellan Areal Camera & Spectrograph (IMACS; Bigelow & Dressler 2003) (Section 2.4) to verify membership via detection of Li I absorption.

## 2.2. Hectochelle

We have observed NGC 2264 with the multi-fiber echelle spectrograph Hectochelle (Szentgyorgyi et al. 1998) on the MMT during several epochs over the past six years. Hectochelle uses robots to position 240 fibers on a  $1^\circ$  field of view (FOV). The fibers subtend  $1''.4$  on the sky yielding a spectral resolution of  $R \sim 35000$ . There are limitations of fiber spacing in a given configuration; no targets may be closer than  $30''$ . We used an order-separating filter (RV31) to cover the wavelength range of  $\sim 5150 - 5300\text{\AA}$ .

The spectra were reduced with an automated pipeline developed by G. Fűrész that utilizes standard spectral reduction procedures within the Image Reduction and Analysis Facility (IRAF)<sup>2</sup>. A more detailed description of Hectochelle data reduction can be found in Sicilia-Aguilar et al. (2006). An additional manual step not taken care of by the pipeline was sky subtraction. A number of fibers ( $\sim 20$ ) must be allocated for sky observations because Hectochelle observations are generally conducted in bright time and the scattered moonlight must be subtracted to measure velocities for faint sources. To subtract the sky observations, we normalized the fiber throughputs using the flat-field exposure, and then subtracted the average spectrum taken from all the sky fibers.

Fűrész et al. (2006) observed NGC 2264 in March 2004 and December 2005; our new observations were conducted in the fall of 2007, 2008, spring 2009, fall 2009, and spring 2010, see Table 1 for details of the observations. When possible two epochs were taken of each field in a particular observing season to identify short period radial velocity variability. Because Hectochelle observations are conducted in queue mode, the second epochs could be days or even a month apart from the first epoch.

---

<sup>2</sup>IRAF is distributed by the National Optical Astronomy Observatories, which are operated by the Association of Universities for Research in Astronomy, Inc., under cooperative agreement with the National Science Foundation.

### 2.3. MIKE Fibers

We also used MIKE Fibers (Bernstein et al. 2003; Walker et al. 2007) on the Magellan Clay telescope to observe NGC 2264 in the spectral range  $\sim 5150 - 5210 \text{ \AA}$ . This instrument uses 256 manually-plugged fibers that fit within a pre-drilled plate on a  $25'$  FOV. Each fiber subtends  $1''.25$  on the sky, resulting in a resolution  $R \sim 18000$  and fibers must be spaced at least  $14''$  apart. MIKE Fibers has two independent spectrograph channels; at  $5200 \text{ \AA}$  we are able to use both channels with 128 fibers going to each channel. The two channels are essentially separate spectrographs with different gratings, optics, and CCDs in the same enclosure.

Because MIKE Fibers has a smaller field of view than Hectochelle, we selected two fields with the highest stellar density for these observations: one in the northern part of the cluster near the O7V star S Mon, and another in the southern part centered between the Spokes and Cone “clusters”. As in the case of the Hectochelle observations, data were taken on two epochs several days apart.

The data were reduced using IRAF. We used the task *ccdproc*, to carry out initial reductions on the raw CCD imaging data: subtracting the overscan, trimming, and subtracting the bias. We combined our individual exposures with ‘imcombine’ set for cosmic ray rejection. The spectra were extracted using ‘twospec’, by first tracing the apertures in a flat field frame taken of a continuum source to create a map of aperture traces to extract the science spectra. The wavelength solution was calibrated by fitting a 4th order Legendre polynomial to the Thorium-Argon (Th-Ar) lamp spectrum taken before and after the sets of science observations.

### 2.4. IMACS spectra

Low-resolution spectra for the purpose of determining membership from Li I  $6707 \text{ \AA}$  absorption were obtained with IMACS on the Magellan Baade telescope, during December 20-22 2010 (UT). The setup was the same as used in our study of the L1641 region of the Orion A cloud (Hsu et al. 2012). We used the IMACS f/2 camera in multi-slit spectroscopy mode with the 300 line grism at a blaze angle of  $17.5^\circ$ . With a  $0''.6$  slit, this configuration yields a resolution of  $4 \text{ \AA}$  and spectral coverage from approximately  $4000 \text{ \AA}$  to  $9000 \text{ \AA}$ . The standard observation time for each field is  $5 \times 10$  minutes, but we increased the time to  $6 \times 10$  minutes for a few observations at higher airmasses. A total of 160 stars were observed, selected primarily from the stars that appear slightly blueshifted from the gas (see Section 3 and 4.2).

### 2.5. Radial velocity measurements

We used *rvsao* package in IRAF (Mink & Kurtz 1998), to measure the radial velocities of our observed targets. The radial velocity of an object is determined by cross-correlating the observed

spectrum with a template spectrum of known velocity. The cross-correlation signal-to-noise (S/N) or quality is given by  $R$ , defined as

$$R = \frac{h}{2^{1/2}\sigma_a} \quad (1)$$

where  $h$  is the peak height of the correlation function and  $\sigma_a$  is the rms noise estimated from the antisymmetric portion of the correlation function. The velocity measurement error also depends on the spectral resolution; it is of the form

$$\sigma_v \sim \frac{C}{1 + R} \quad (2)$$

where  $C$  is 20 km s<sup>-1</sup> for MIKE Fibers and 14 km s<sup>-1</sup> for Hectochelle. These values were determined empirically by adding random noise to a high S/N spectrum as in Hartmann et al. (1986).

We used libraries of synthetic stellar spectra as velocity templates rather than observed velocity standards, enabling us to explore a wider range of stellar parameters than a few observed templates. We used the library by Coelho et al. (2005) for velocity measurement of spectra from both Hectochelle and MIKE Fibers. The Coelho et al. (2005) templates are computed with a resolution of  $R \sim 100,000$ , much higher resolution than the observed spectra. However, a cosine-bell filter function is applied to the Fourier transform of the template and observed spectrum within the *xcsao* task. This effectively reduces the template resolution to that of the Hectochelle or MIKE Fibers instrument. The filter applied to the data from both instruments (and templates) has an inner cutoff at a wave number of 10 and the filter function increases to 1 at a wave number of 40. The purpose of the inner cutoff is to limit the effect of large-scale features in the cross-correlation. The outer cutoff values depend on the instrument and limit on the smallest features considered in the cross-correlation. Tonry & Davis (1979) suggests an outer cutoff of  $\sim N_{pixels}/(2\pi \times \text{FWHM}/2.355)$ , yielding  $\sim 400$  for Hectochelle and  $\sim 80$  for MIKE Fibers. However, we found that outer wavenumber cutoff beginning at 120 and reaching zero at 450 worked the best for MIKE Fibers and a cutoff beginning at 600, reaching zero at 1000 worked best for Hectochelle.

We used a subset of the spectral templates with surface gravity  $\log(g) = 3.5$ , effective temperatures ( $T_{eff}$ ) ranging from 3500 - 7000K in steps of 250K, and solar metallicity. There was no need to explore a wider parameter space with the templates because the most important factor determining the quality of a correlation was the  $T_{eff}$  of the template.

The results from the correlation with the highest  $R$  value are selected, matched to the appropriate target coordinates, and stored in a Starbase database (Roll 1996). The right ascension and declination are used to correlate the new observations with the existing catalog and the coordinates are used to generate a truncated 2MASS ID number (2MASSID), throwing out fractional seconds in right ascension and declination. Once the targets have been matched in right ascension and declination, the 2MASSID is used to identify sources in further analysis.

To combine radial velocities taken in different epochs, it is necessary to determine zeropoint velocity shifts for an entire observation. This compensates for possibly different calibration schemes,

different wavelengths, different instruments, as well as temperature variations within the spectrograph (Sicilia-Aguilar et al. 2006; Fűrész et al. 2006, 2008). We also accounted for the well-characterized fiber-to-fiber velocity offset caused by the calibration lamps not illuminating the fibers in the same way as astronomical objects.

We adopted the results of Fűrész et al. (2006) as baseline velocities to shift our observations to match. This is because the Fűrész et al. (2006) velocities are referenced to the radial velocity standard star W23870 (Latham et al. 1991), having an absolute velocity accuracy of  $\pm 0.2 \text{ km s}^{-1}$  (Stefanik et al. 1999). We applied a constant shift for each field given by the mean of a Gaussian fit to the distribution of radial velocity differences for each target in a field. The zeropoint shifts for the Hectochelle and MIKE Fibers fields are generally quite small, less than  $0.5 \text{ km s}^{-1}$  and are given in Tables 1 and 2. In contrast, observations of the ONC in Tobin et al. (2009) had zeropoint shifts  $\sim 1 \text{ km s}^{-1}$ . Given that many NGC 2264 fields were conducted in the same semester and even same nights as the Orion fields, the zeropoint shifts may be overestimated in Tobin et al. (2009). We believe that the NGC 2264 fields track the zeropoint shift better than the Orion fields due to the inclusion of many bright non-members in the Galactic Plane that give velocity precisions of  $0.5\text{-}0.2 \text{ km s}^{-1}$  (note that this is the formal error and does not include systematic effects.)

We have converted the heliocentric radial velocities of each target to the kinematic local standard of rest (LSR) velocities (Kerr & Lynden-Bell 1986). In order to compare the velocity structure of the stars and gas, the LSR velocities are used exclusively in the plots, but the heliocentric radial velocities are given in Table 3.

The multi-epoch observations have enabled us to also identify a number of candidate spectroscopic binaries from radial velocity variability and/or double-peaked correlation functions. We have removed these from the cluster kinematic analysis because they will broaden the cluster velocity distribution. These candidate spectroscopic binaries will be presented in a subsequent paper along with observations from later epochs.

## 2.6. Li and spectral types

Spectral types and Li I 6707 Å absorption equivalent widths were determined for a subset of target stars observed with IMACS. We used SPTCLASS, a semi-automatic spectral-typing program (Hernández et al. 2004), which uses empirical relations of spectral type and absorption line equivalent widths for classification (see Hsu et al. (2012) for details). SPTCLASS also automatically measures Li I equivalent widths, but we made manual determinations because of the uncertainty in automatically setting continuum levels at this resolution when strong TiO bands are present.

### 3. Results

The combined radial velocity measurements from our observations are presented in Table 3. Of the 695 stars with measured non-variable radial velocities, approximately 407 are probable members based on their radial velocities, with more certain identification for those objects with IR excess and/or Li I absorption. This approximately doubles the number of stars with radial velocities (excluding spectroscopic binaries) available in the previous study of (Paper I).

Figure 1 shows an overview of the spatial and kinematic properties of our sample and its correlation with the molecular gas in the region. The left panel shows the positions of all the radial velocity targets overplotted on the corresponding  $^{13}\text{CO}$  intensity map from Ridge et al. (2006) for comparison. In the right panel, we show the position-velocity (PV) distribution of the stars summed over right ascension and plotted as function of declination to correspond roughly to the long axis of the cluster, with the corresponding  $^{13}\text{CO}$  PV plot. Targets that show infrared (IR) excess emission, as defined by  $K_s - [3.6] > 0.4$  and  $[3.6] - [4.5] > 0.2$ , where  $K_s$  is from 2MASS and the other colors are IRAC bands 1 and 2, are marked as filled stars; targets with detectable Li absorption but no IR excess are shown as open stars.

The spatial and kinematic correlations between stellar members and molecular gas are evident. The targets with projected spatial positions well off the main molecular gas emission are mostly taken with Hectochelle, chosen to use “left-over” fibers; these are largely non-members, as expected, based on their radial velocities that differ substantially from the cluster mean.

Figure 2 focuses on the same comparisons between stars and gas in more detail by removing stars with LSR velocities  $< -2 \text{ km s}^{-1}$  and  $> 15 \text{ km s}^{-1}$ . The overall kinematic properties of the stars are similar to that found by Fűrész et al. (2006) (compare the right panel of their Figure 6), but by approximately doubling the number of members with radial velocity measurements several aspects become much clearer. First, the addition of many new members in the region of the Spokes Cluster (Teixeira et al. 2006) at  $\delta \sim 9.6^\circ$ , RA  $\sim 100.25^\circ$  shows a substantial velocity dispersion with an extension to blueshifted velocities, corresponding to a similar feature in the  $^{13}\text{CO}$  emission between  $2 \text{ km s}^{-1}$  and  $5 \text{ km s}^{-1}$ . Second, the population of redshifted stars in the north corresponding to the molecular gas component at  $V(\text{lsr}) \sim 10 \text{ km s}^{-1}$  is better defined; there appears to be a gap at  $\delta \sim 9.85$ ,  $V(\text{lsr}) \sim 7 \text{ km s}^{-1}$  in both distributions. Finally, there is a “blueshifted population with velocities  $-2 \text{ km s}^{-1} \lesssim V(\text{lsr}) \lesssim 2 \text{ km s}^{-1}$  which does not have corresponding  $^{13}\text{CO}$  emission and was not apparent in Fűrész et al. (2006).

To further examine the velocity distributions relative to the gas, we have plotted histograms of the stellar and gas velocities in Figure 3 in the noted declination bins. We only include a range of RA between  $100.05^\circ$  and  $100.4^\circ$  to focus on the main cluster and limit the contribution of the dispersed population. The histograms show that while there is a strong overlap in velocity space between stars and molecular gas, there is a modest but significant population of blueshifted stars which do not have associated  $^{13}\text{CO}$  emission at their velocity. A substantial fraction of these blueshifted stars show either infrared excess or strong Li I absorption (Figure 2), indicating that

they are not substantially older foreground objects. Moreover, contamination by field stars (for which we do not have either Li measurements or observed infrared excess) is unlikely to have a major effect on this distribution; we estimate a contamination of  $\sim 13$  non-members in Figure 3. We determine this number by counting the number of stars with velocities between  $-35 \text{ km s}^{-1} < V(\text{l sr}) < -5 \text{ km s}^{-1}$  and  $20 \text{ km s}^{-1} < V(\text{l sr}) < 50 \text{ km s}^{-1}$  in the same range of right ascension and assuming a uniform distribution in radial velocity.

The other obvious feature of note is the redshifted population of stars at  $9.8^\circ < \delta < 10^\circ$  (Figure 2). This group corresponds in velocity space to a corresponding clump of  $^{13}\text{CO}$  emission at  $7 \text{ km s}^{-1} < V(\text{l sr}) < 12 \text{ km s}^{-1}$ . There is a gap or minimum in the CO emission at  $V(\text{l sr}) \sim 7 \text{ km s}^{-1}$ , and **there is an indication of a similar minimum in the stellar velocity distribution, though it is statistically insignificant** (Figure 3). We suggest that this structure is the result of the strong wind of S Mon driving a bubble into the molecular gas, triggering star formation as the gas is compressed.

The histogram of the full sample with in a RA range of  $100.05^\circ$  and  $100.4^\circ$  and a Dec. range of  $9.35^\circ$  to  $10.0^\circ$  is shown in the bottom panel of Figure 3. We fit a Gaussian to this histogram and derive a velocity dispersion of  $2.8 \text{ km s}^{-1}$ . We account for the average velocity error of  $1.2 \text{ km s}^{-1}$  for the stars used in the calculation by subtracting this error in quadrature from the velocity dispersion and the corrected velocity dispersion is then  $2.5 \text{ km s}^{-1}$ .

Figure 4 provides another view of the cluster structure in terms of position-velocity maps, but by stepping across the cluster in  $0.1^\circ$  swaths of RA. The symbols have the same meaning as in Figure 2, but they are now color-coded to emphasize blue- and red-shifted populations. Here we call attention to the small group of stars shown in the bottom left panel (RA = 100.4 to 100.5) centered around  $V(\text{l sr}) \sim 2 \text{ km s}^{-1}$ ,  $\delta \sim 9.5^\circ$  and not associated with  $^{13}\text{CO}$  emission. Only one of these stars exhibits infrared excess, suggesting that this might be a slightly older group; on the other hand, many show Li absorption. The population blueshifted stars is apparent in nearly all RA bins across the cluster.

## 4. Discussion

### 4.1. Kinematics and gravitational binding

The overall kinematic structure of NGC 2264 bears a striking similarity to that found in the Orion Nebula Cluster (ONC). As shown in Figure 3 of Tobin et al. (2009), the position-velocity plot of both stars and gas shows a northern region redshifted with respect to the central region. The right panel of Figure 2 shows qualitatively similar behavior, although more clearly in the gas than in the stars. One also observes the same asymmetry between the stellar and gas velocities, with a population of stars blueshifted with respect to the molecular gas. The 1-dimensional velocity dispersions of the two clusters are also similar,  $\sigma = 3.1 \text{ km s}^{-1}$  for Orion (Fűrész et al. 2008) and



$\sigma = 2.5 \text{ km s}^{-1}$  for NGC 2264. NGC 2264 does differ from the ONC with its two components in the molecular gas in the north near S Mon (three if the clump west of S Mon is considered), and the gas in the ONC has only one component. The stars in the northern part of the ONC also have a smaller velocity dispersion with respect to the center of the ONC, while in NGC 2264 the stars in the north have a larger spread in velocity than the northern ONC stars.

Proszkow et al. (2009) suggested that the transition from redshifted stars and gas in the northern regions of the ONC to more blueshifted velocities near the cluster center could be the signature of gravitationally-driven infall. The interpretation is qualitatively similar to using “caustics” in position-velocity space to infer gravitational motion in galaxy clusters (e.g., Geller et al. 2013). To see whether a similar interpretation could hold for NGC 2264, we compute a “binding velocity”  $v_b \sim (2GM/r)^{1/2}$ . Crutcher et al. (1978) estimated a total gas mass of  $\sim 8000 M_\odot$  spanning a total length of  $\sim 10 \text{ pc}$ . Using this mass and setting  $r \sim 5 \text{ pc}$  yields  $v_b \sim 3.6 \text{ km s}^{-1}$ .

However, while this scenario was plausible for Orion, it seems less likely to explain the redshifted population in the north of NGC 2264. This group has  $V(\text{lsr}) \sim 10 \text{ km s}^{-1}$  which is redshifted by about  $5 \text{ km s}^{-1}$  with respect to the gas and stellar velocities at the position of the Spokes Cluster. Unless the gas mass (which is the dominant contributor) is underestimated by roughly a factor of four, it seems very likely that this redshifted population is not bound to the rest of the cloud. Rather, we suggest this group is more likely to be the result of blowout by the wind from S Mon; this would also explain the “hole” in the gas at  $\delta \sim 9.8^\circ$ ,  $V(\text{lsr}) \sim 7 \text{ km s}^{-1}$ .

With respect to the rest of the cluster, the binding velocity calculated from the molecular gas is larger than the 1-dimensional velocity dispersion ( $\sigma_v = 2.5 \text{ km s}^{-1}$ ) within a restricted range of RA (bottom right panel of Figure 3). However, if the velocity dispersion is isotropic, the 3-dimensional velocity dispersion would be  $\sim 4.3 \text{ km s}^{-1}$  and thus suggests that the region is unbound. In addition, if our suggestion that a redshifted population is missing from our optical sample is correct, the 1-d velocity dispersion of the total stellar population is larger than we measure here. Resolution of these question will wait until we have proper motions from Gaia. For now, we conjecture that the true situation is a mix of possibilities, with some fraction of the stars that will eventually be left behind in a bound cluster and some dispersing.

## 4.2. Blueshifted population

As discussed in the previous section, it appears that a substantial fraction of the blueshifted stars are causally-related to NGC 2264 if not members, based on the indicators of youth - infrared excesses and Li absorption. One possibility for explaining why this population is not at the same velocity as the molecular gas is that it might be older, resulting from a previous episode of star formation. To test this idea, we constructed color-magnitude diagrams for the various kinematic groups. As seen in Figure 5, the color magnitude diagram (CMD) of the “field” stars with velocities  $< -5 \text{ km s}^{-1}$  and  $> 18 \text{ km s}^{-1}$  from the cluster mean shows a much larger dispersion around the

median color-magnitude line of the cluster. We observed an excess of faint stars, as would be expected for foreground main sequence stars, and brighter, redder background giants. Moreover, the blue-shifted stars tend to be brighter and bluer in color, while the red-shifted stars are fainter, redder, and have more dispersion in magnitude.

The CMDs of the various probable cluster member velocity groups are essentially indistinguishable except for the redshifted group with  $8 \text{ km s}^{-1} < V(lsr) < 15 \text{ km s}^{-1}$ , which exhibits a broader dispersion. This could be due to contamination **because the northern region, where much of the  $8 \text{ km s}^{-1} < V(lsr) < 15 \text{ km s}^{-1}$  population is found,** has less extinction to cut out background stars (and is also sparser). The blue-shifted group ( $-2 \text{ km s}^{-1} < V(lsr) < 2 \text{ km s}^{-1}$ ) appears to have a larger fraction of redder stars than the main cluster as well. However, because these photometric data have not been de-reddened, it is impossible to decouple evolutionary effects or population differences from extinction. Notice that the reddening vector shown in Figure 5 is nearly parallel to the median CMD of the cluster. On the whole, there is a significant spread in  $V$  at a given  $V - I_C$  color, but much of this is undoubtedly due to an unresolved binary population; other sources of error are probably present but poorly-understood (Jeffries 2012). In any case, there is little evidence for any systematic age differences larger than about  $\sim 2 - 3$  Myr, comparable to the median estimated age of the cluster (Sung & Bessell 2010).

Systematic ejection of stars toward Earth seems unlikely if not implausible, especially because the ONC shows the same excess of blueshifted stellar velocities relative to the molecular gas velocities. We next consider other possibilities for the asymmetry between the stellar and gas velocities. The first possibility recognizes that we have an optically-biased sample of radial velocities; stars moving away from us would move more deeply into the molecular cloud and thus have much higher line-of-sight extinctions. It seems very likely that some bias exists; as shown in Figure 3, we observe relatively few stars at the reddest velocities of the molecular gas, which would be surprising if not attributable to sample bias. Whether there exists a substantial population of redshifted stars with velocity shifts of comparable magnitude to the blueshifted population is not clear. If such a population did exist, the overall velocity dispersion would increase to  $\sigma_v \sim 5 \text{ km s}^{-1}$ , making it even less likely that any part of the region is gravitationally-bound.

An alternative possibility to explain the asymmetry between stars and gas is preferential dispersal of blueshifted (nearside) gas by stellar energy input. We argued above that S Mon is blowing away gas, producing the “hole” in the  $^{13}\text{CO}$  emission at  $\sim 7 \text{ km s}^{-1}$ ,  $\delta \sim 9.8^\circ$ . It seems conceivable that this O7 star could have dispersed additional molecular gas. Schwartz et al. (1985) argued that S Mon is responsible for photoionizing the rim of the Cone Nebula at a projected distance of about 6 pc. Furthermore, they argued that S Mon and the Cone Nebula might actually lie a substantial distance in the foreground from other dense molecular gas in the region (basically, the Spokes Cluster region). Whether or not this picture is correct, it is possible that S Mon photoevaporated and photoionized the gas originally on the near side of the original molecular cloud.

The simulations of photodissociation and ionization of initially molecular gas with magnetic

fields and turbulence by Arthur et al. (2011) show substantial evacuation of a region of size 4 pc and initial density  $n = 10^3 \text{cm}^{-3}$  in only  $4 \times 10^5$  yr for an assumed O9 star, which emits a factor of 3 – 4 fewer ionizing photons than an O7 star is expected to provide (Osterbrock & Ferland 2006, Table 2.3). Thus, it is possible that there had been an episode of star formation in the near side of the molecular cloud, prior to the formation of S Mon. Once S Mon formed and began photoionizing the molecular gas associated with the previous generation of star formation, the molecular gas removal caused the previously formed stars to become unbound and expand (e.g., Lada & Lada 2003). This scenario would produce a population of stars systematically blue-shifted with respect to the cloud velocity, because we are able to observe the blue-shifted stars due to their low extinction, but the red-shifted stars move into the molecular cloud and become too extinguished to determine radial velocities in the optical. We therefore suggest that the observed kinematic differences between the stellar population and the molecular gas result from a combination of optical bias against stars moving into the molecular gas and blowout of molecular gas on the near side by S Mon. The low extinction observed toward some members (Walker 1956; Park et al. 2000) is clear evidence for some gas dispersal to have taken place.

While we cannot determine a systematic age difference between the blue-shifted population and the rest of the cluster, Sung & Bessell (2010) argued that the ‘field’ and ‘halo’ populations of NGC 2264 are older than the rest of the cluster. These regions are designated as such because they are spread across the NGC 2264 region on the sky and the blue-shifted population of stars is found at all positions in NGC 2264 (see Figure 4). It is noteworthy that Orion also has several known foreground populations as well, projected on the same region of the sky as the ONC (e.g., Bally 2008; Alves & Bouy 2012), possibly contributing to the blue-shifted population observed there.

## 5. Summary

The comparison of the spatial-kinematic properties of stars and molecular gas suggests that NGC 2264 may be better understood as a loose collection of star-forming clumps rather than as a single, distinct, strongly-bound cluster. Future astrometric surveys to determine distances and proper motions are needed to fully develop the true picture of this object.

We wish to thank the anonymous referee for comments which improved the clarity of the manuscript. The authors wish to thank the staff of the MMT and Magellan telescopes and the Hectochelle queue observers of 2007, 2008, 2009, and 2010 for their efforts in obtaining the data used in this paper. We also thank M. Walker and E. Olszewski for assistance with MIKE Fibers data acquisition/reduction and Jesus Hernandez for useful discussions. J. T. and L. H. acknowledge funding from NSF grant AST 08070305. J.J.T. acknowledges support provided by NASA through Hubble Fellowship grant #HST-HF-51300.01-A awarded by the Space Telescope Science Institute, which is operated by the Association of Universities for Research in Astronomy, Inc., for NASA, under contract NAS 5-26555. This research has made use of NASA’s Astrophysics Data System. The National Radio Astronomy Observatory is a facility of the National Science Foundation operated

under cooperative agreement by Associated Universities, Inc.

*Facilities:* Spitzer (IRAC), Magellan:Clay (MIKE), MMT (Hectochelle)

## REFERENCES

- Allen, L., et al. 2007, *Protostars and Planets V*, 361
- Alves, J., & Bouy, H. 2012, *A&A*, 547, AA97
- Arthur, S. J., Henney, W. J., Mellema, G., de Colle, F., & Vázquez-Semadeni, E. 2011, *MNRAS*, 414, 1747
- Bernstein, R., Shectman, S. A., Gunnels, S. M., Mochmacki, S., & Athey, A. E. 2003, *Proc. SPIE*, 4841, 1694
- Bally, J., Langer, W. D., Wilson, R. W., Stark, A. A., & Pound, M. W. 1991, *Fragmentation of Molecular Clouds and Star Formation*, 147, 11
- Ballesteros-Paredes, J., Hartmann, L., & Vázquez-Semadeni, E. 1999, *ApJ*, 527, 285
- Bally, J. 2008, *Handbook of Star Forming Regions, Volume I*, 459
- Baraffe, I., Vorobyov, E., & Chabrier, G. 2012, *ApJ*, 756, 118
- Bate, M. R. 2012, *MNRAS*, 419, 3115
- Baxter, E. J., Covey, K. R., Muench, A. A., Fűrész, G., Rebull, L., & Szentgyorgyi, A. H. 2009, *AJ*, 138, 963
- Bigelow, B. C., & Dressler, A. M. 2003, *Proc. SPIE*, 4841, 1727
- Bonnell, I. A., Bate, M. R., & Vine, S. G. 2003, *MNRAS*, 343, 413
- Carpenter, J. M. 2000, *AJ*, 120, 3139
- Coelho, P., Barbuy, B., Meléndez, J., Schiavon, R. P., & Castilho, B. V. 2005, *A&A*, 443, 735
- Cottar, M., et al. 2014, *A&A*, submitted
- Crutcher, R. M., Hartkopf, W. I., & Giguere, P. T. 1978, *ApJ*, 226, 839
- Dahm, S. E. 2008, *Handbook of Star Forming Regions, Volume I*, 966
- Feigelson, E. D., Townsley, L. K., Broos, P. S., et al. 2013, *ApJS*, 209, 26
- Foster, J. B., Cottar, M., Covey, K. R., et al. 2014, arXiv:1411.6013
- Fűrész, G., et al. 2006, *ApJ*, 648, 1090
- Fűrész, G., Hartmann, L. W., Megeath, S. T., Szentgyorgyi, A. H., & Hamden, E. T. 2008, *ApJ*, 676, 1109
- Geller, M. J., Diaferio, A., Rines, K. J., & Serra, A. L. 2013, *ApJ*, 764, 58
- Hartmann, L. 2009, *Accretion Processes in Star Formation: Second Edition*, Cambridge University Press
- Hartmann, L., Hewett, R., Stahler, S., & Mathieu, R. D. 1986, *ApJ*, 309, 275
- Hartmann, L., Ballesteros-Paredes, J., & Bergin, E. A. 2001, *ApJ*, 562, 852
- Hartmann, L., & Burkert, A. 2007, *ApJ*, 654, 988

- Hernández, J., Calvet, N., Briceño, C., Hartmann, L., & Berlind, P. 2004, *AJ*, 127, 1682
- Hsu, W.-H., Hartmann, L., Allen, L., et al. 2012, *ApJ*, 752, 59
- Jeffries, R. D. 2012, *Star Clusters in the Era of Large Surveys*, 163
- Kerr, F. J., & Lynden-Bell, D. 1986, *MNRAS*, 221, 1023
- Krumholz, M. R., Klein, R. I., & McKee, C. F. 2011, *ApJ*, 740, 74
- Krumholz, M. R., Bate, M. R., Arce, H. G., et al. 2014, arXiv:1401.2473
- Lada, C. J., & Lada, E. A. 2003, *ARA&A*, 41, 57
- Latham, D. W., Davis, R. J., Stefanik, R. P., Mazeh, T., & Abt, H. A. 1991, *AJ*, 101, 625
- Mink, D. J., & Kurtz, M. J. 1998, *Astronomical Data Analysis Software and Systems VII*, 145, 93
- Osterbrock, D. E., & Ferland, G. J. 2006, *Astrophysics of gaseous nebulae and active galactic nuclei*, 2nd. ed.. Sausalito, CA: University Science Books
- Park, B.-G., Sung, H., Bessell, M. S., & Kang, Y. H. 2000, *AJ*, 120, 894
- Proszkow, E., Adams, F. C., Hartmann, L., & Tobin, J. J. 2009, *ApJ* in press.
- Ramírez, S. V., et al. 2004, *AJ*, 127, 2659
- Rebull, L. M., et al. 2002, *AJ*, 123, 1528
- Ridge, N. A., et al. 2006, *AJ*, 131, 2921
- Roll, J. 1996, *Astronomical Data Analysis Software and Systems V*, 101, 536
- Schwartz, P. R., Thronson, H. A., Jr., Odenwald, S. F., et al. 1985, *ApJ*, 292, 231
- Shu, F. H., Adams, F. C., & Lizano, S. 1987, *ARA&A*, 25, 23
- Sicilia-Aguilar, A., Hartmann, L. W., Fűrész, G., Henning, T., Dullemond, C., & Brandner, W. 2006, *AJ*, 132, 2135
- Skiff, B. A. 2013, *VizieR Online Data Catalog*, 1, 2023
- Stefanik, R. P., Latham, D. W., & Torres, G. 1999, *IAU Colloq. 170: Precise Stellar Radial Velocities*, 185, 354
- Sung, H., Bessell, M. S., & Lee, S.-W. 1997, *AJ*, 114, 2644
- Sung, H., Bessell, M. S., Chun, M.-Y., Karimov, R., & Ibrahimov, M. 2008, *AJ*, 135, 441
- Sung, H., Stauffer, J. R., & Bessell, M. S. 2009, *AJ*, 138, 1116
- Sung, H., & Bessell, M. S. 2010, *AJ*, 140, 2070
- Szentgyorgyi, A. H., Cheimets, P., Eng, R., Fabricant, D. G., Geary, J. C., Hartmann, L., Pieri, M. R., & Roll, J. B. 1998, *Proc. SPIE*, 3355, 242
- Tan, J. C., Krumholz, M. R., & McKee, C. F. 2006, *ApJ*, 641, L121
- Teixeira, P. S., Lada, C. J., Young, E. T., et al. 2006, *ApJ*, 636, L45
- Tobin, J. J., Hartmann, L., Furesz, G., Mateo, M., & Megeath, S. T. 2009, *ApJ*, 697, 1103

Tonry, J., & Davis, M. 1979, *AJ*, 84, 1511

Walker, M. G., Mateo, M., Olszewski, E. W., Bernstein, R., Sen, B., & Woodroffe, M. 2007, *ApJS*, 171, 389

Walker, M. F. 1956, *ApJS*, 2, 365

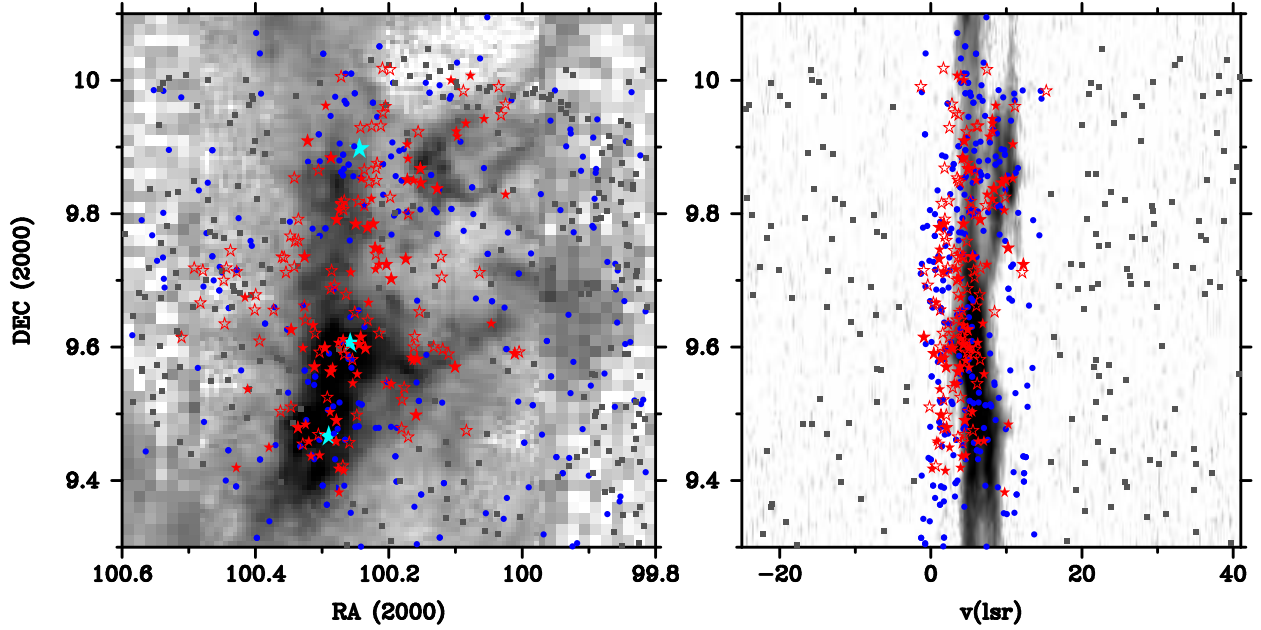


Fig. 1.— NGC 2264 radial velocity targets superimposed on the  $^{13}\text{CO}$  integrated intensity map (grayscale) from Ridge et al. (2006) (left panel) and the radial velocity targets are overlaid on a position-velocity plot (right panel) summing over the RA range in the left panel. The lower resolution portion at the edges of the left panel is from J. Bally (unpublished). Star symbols represent members as determined from IRAC infrared excesses (filled stars) or the detection of Li I absorption (open stars); blue circles denote non-excess stars that were not observed for Li absorption, but whose velocities  $-2 \text{ km s}^{-1} < V(lsr) < 15 \text{ km s}^{-1}$  suggest possible membership. Gray squares represent stars with LSR velocities  $< -2$  and  $> 15 \text{ km s}^{-1}$  that are unlikely to be cluster members. The non-members (gray squares) are roughly distributed uniformly in velocity and declination. From north to south, the cyan stars in the left panel correspond to the position of S Mon, the Spokes Cluster center, and the Cone cluster center.

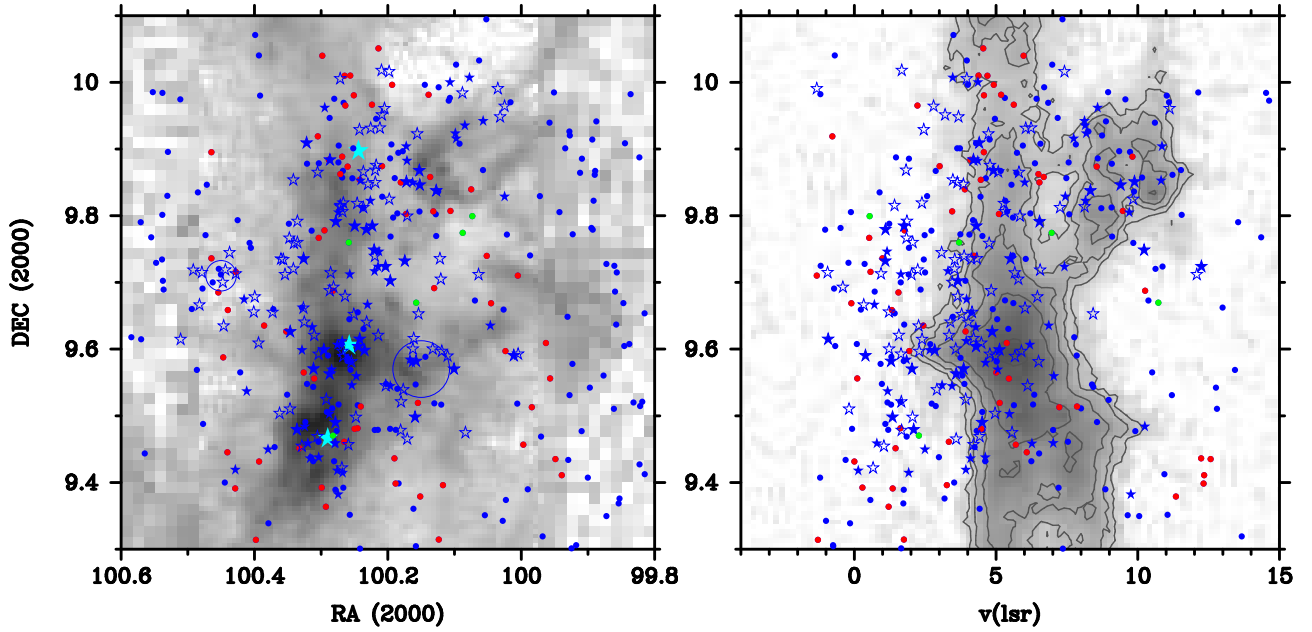


Fig. 2.— Radial velocities of known and likely members again superimposed upon the  $^{13}\text{CO}$  integrated intensity map, as in Figure 1 projected spatially (left) and in the declination position-velocity map (right). Symbol shapes are the same as in Figure 1 - filled stars for infrared-excess stars, open stars for Li absorption detections, and filled circles for possible members that do not have infrared-excess (or lack photometry) and/or Li absorption measurements. The red circles are sources without an infrared-excess excess and do not have IMACS observations to detection Li absorption. The green circles are sources without infrared-excess, have IMACS observations. The large open circles highlight two regions that show a clustering of blue-shifted stars. From north to south, the cyan stars in the left panel correspond to the position of S Mon, the Spokes Cluster center, and the Cone cluster center.



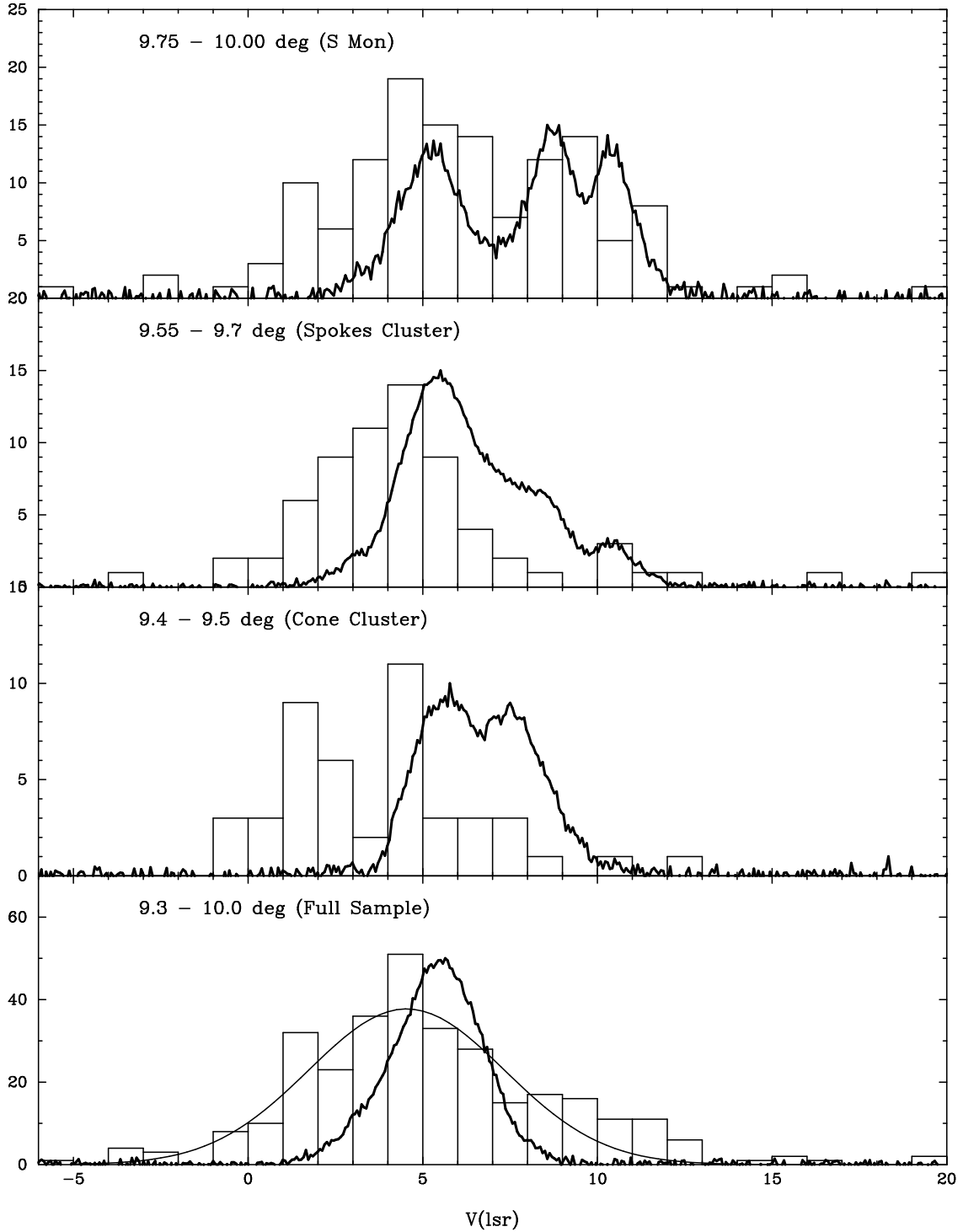


Fig. 3.— RV histograms for stars and gas (thick line) for selected bins in declination. Note the systematic blue shift of the stellar distribution compared to the gas in the southern part of the cluster. The smooth curve in the bottom panel is a Gaussian fit to the stellar RV histogram, yielding a one-dimensional velocity dispersion of  $\sigma = 2.8 \text{ km s}^{-1}$ ; after accounting for the average error of  $1.2 \text{ km s}^{-1}$ , the velocity dispersion is reduced to  $2.5 \text{ km s}^{-1}$ . Note that we only plot stars with RA between 100.4 and 100.05 to focus on the main cluster area and limit contamination.

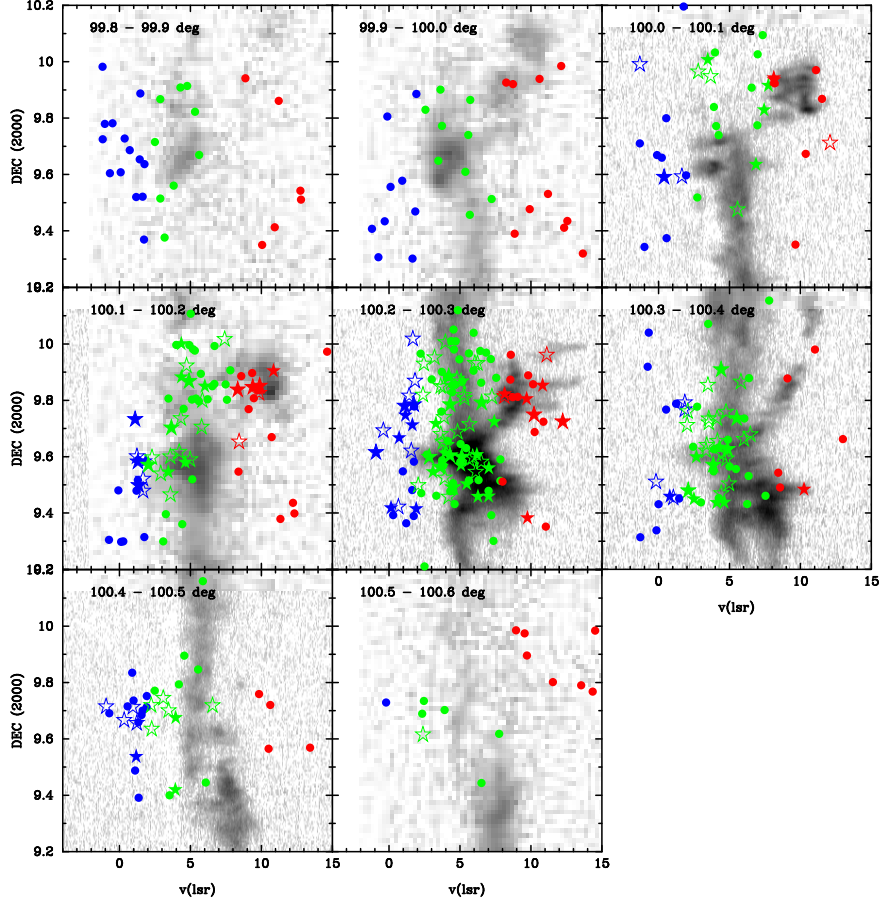


Fig. 4.— PV plots for different bins in RA across the cluster. Important to note are the 100.2 to 100.4 bins which show that moving north in the cluster there are three distinct velocity components. The blue points are used for stars with  $V(\text{lsr}) \leq 2 \text{ km s}^{-1}$ , the green points are used for stars with  $2 \text{ km s}^{-1} < V(\text{lsr}) < 8 \text{ km s}^{-1}$ , and the red points are used for stars with  $V(\text{lsr}) \geq 8 \text{ km s}^{-1}$ .

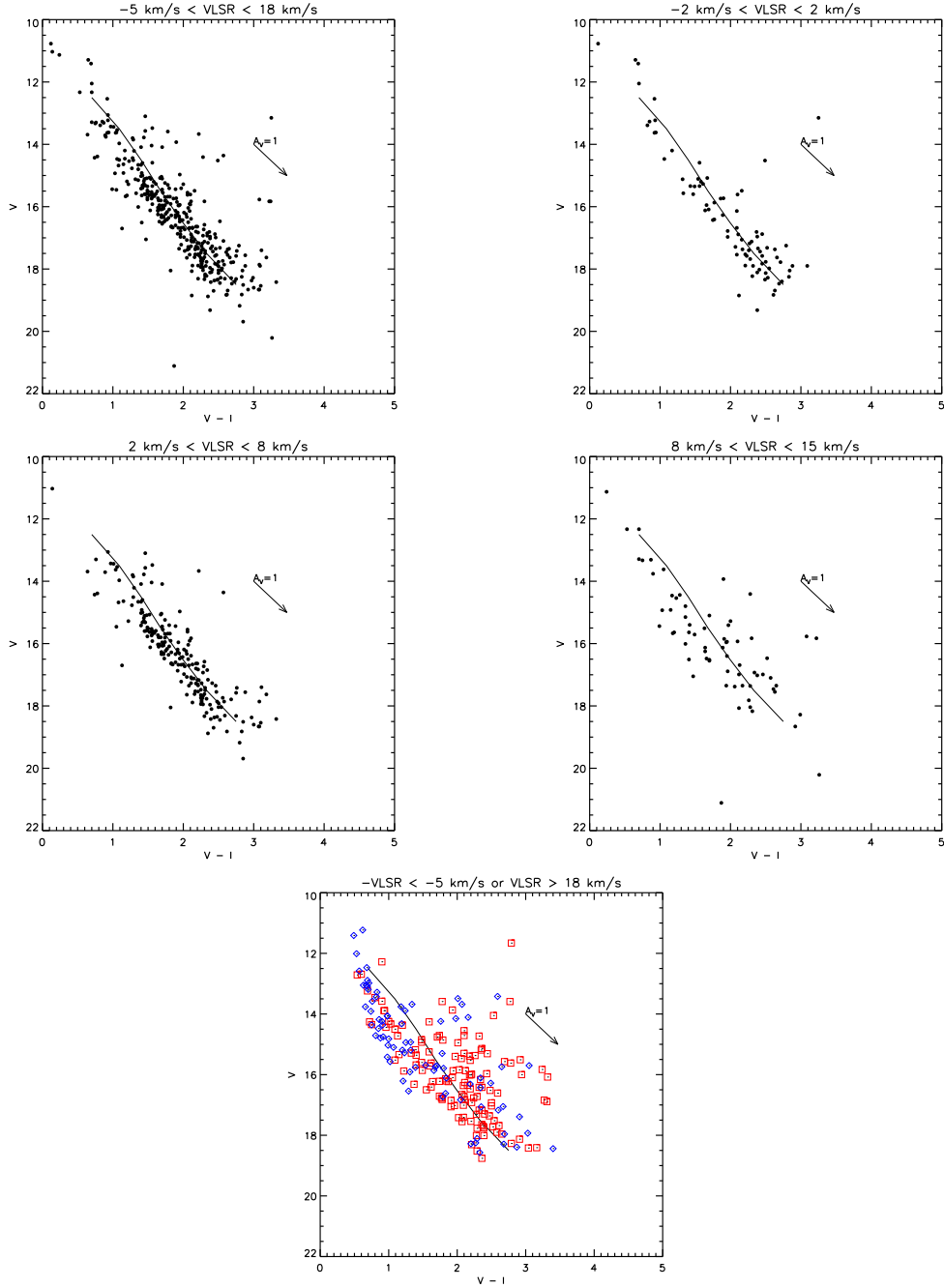


Fig. 5.— Optical color magnitude diagrams of our NGC 2264 targets with optical photometry from Rebull et al. (2001); the photometry are not corrected for extinction. The top left panel is the CMD of stars with radial velocity that is consistent with cluster membership,  $-5.0 \text{ km s}^{-1} < V(\text{l sr}) < 18.0 \text{ km s}^{-1}$ . The top right panel shows stars within the group that is blue-shifted of the gas velocity  $-2.0 \text{ km s}^{-1} < V(\text{l sr}) < 2.0 \text{ km s}^{-1}$ . The middle left panel shows stars with the main cluster velocity,  $2.0 \text{ km s}^{-1} < V(\text{l sr}) < 8.0 \text{ km s}^{-1}$ . The middle right panel shows stars that a redshifted of the main cluster  $8.0 \text{ km s}^{-1} < V(\text{l sr}) < 15.0 \text{ km s}^{-1}$ . The bottom panel shows stars that are anti-correlated with the cluster velocity; the blue or red boxes denote whether the stars is significantly blue or red-shifted away from the cluster velocity. The *solid line* in both panels is the median V-I color for stars with velocities consistent with NGC 2264. The CMDs of the three groups within the cluster velocity are all consistent with each other, showing that they are at similar distances and ages. The stars outside the main cluster velocities show a significantly different CMD that is comprised of both foreground and background sources.

Table 1. Hectochelle Observations

Field ID	Date UT Date	Julian Date (2400000)	RA (J2000)	Dec. (J2000)	Airmass	Exposure Time # × seconds	Binning	Filter	Zeropoint Shift <sup>a</sup> km s <sup>-1</sup>	Number of Targets	Seeing arcsec
F1-E1-2007	10-12-2007	54385.42	06:40:57.74	09:40:26.20	1.33	3x1200	2x2	RV31	-0.18 ± 0.02	147	1.07
F1-E2-2007	10-26-2007	54399.42	06:40:57.74	09:40:26.20	1.19	3x1200	2x2	RV31	+0.23 ± 0.02	147	0.64
F2-E1-2007	10-12-2007	54385.48	06:40:39.15	09:45:23.48	1.12	3x1200	2x2	RV31	-0.08 ± 0.04	147	0.61
F2-E2-2007	10-28-2007	54401.40	06:40:39.15	09:45:23.48	1.25	3x1200	2x2	RV31	+0.23 ± 0.03	147	1.4
F3-E1-2007	10-29-2007	54402.44	06:41:06.09	09:42:34.69	1.12	3x1200	2x2	RV31	-0.02 ± 0.02	144	1.97
F3-E2-2007	11-25-2007	54429.40	06:41:06.09	09:42:34.69	1.08	3x1200	2x2	RV31	-0.18 ± 0.08	144	2.32
F4-E1-2007	10-29-2007	54402.49	06:40:51.25	09:33:13.59	1.08	1x1200	2x2	RV31	+0.14 ± 0.04	143	1.97
F1-E1-2008	10-22-2008	54761.49	06:40:46.44	09:37:36.39	1.08	3x1200	2x2	RV31	-0.30 ± 0.02	138	1.38
F1-E2-2008	10-26-2008	54765.42	06:40:46.44	09:37:36.39	1.19	3x1200	2x2	RV31	-0.30 ± 0.03	138	0.82
F2-E1-2008	10-24-2008	54763.46	06:40:53.44	09:47:21.13	1.10	3x1200	2x2	RV31	-0.10 ± 0.04	147	0.64
F2-E2-2008	10-25-2008	54764.44	06:40:53.44	09:47:21.13	1.14	3x1200	2x2	RV31	-0.13 ± 0.04	147	1.02
F3-E1-2008	10-25-2008	54764.48	06:41:02.64	09:42:42.26	1.08	3x1200	2x2	RV31	-0.42 ± 0.03	152	1.02
F4-E1-2008	10-23-2008	54762.45	06:40:46.12	09:32:39.73	1.12	3x1200	2x2	RV31	-0.51 ± 0.05	148	0.95
F1-E1-S2009	03-13-2009	54903.19	06:40:56.18	09:41:16.03	1.20	2x1200	2x2	RV31	-0.37 ± 0.02	191	1.91
F2-E1-S2009	03-14-2009	54904.19	06:40:46.08	09:32:41.51	1.21	4x1200	2x2	RV31	-0.44 ± 0.04	187	1.69
F3-E1-S2009	04-10-2009	54931.14	06:40:39.83	09:45:12.39	1.36	2x1200	2x2	RV31	+0.07 ± 0.03	193	0.67
F3-E2-S2009	04-13-2009	54934.15	06:40:39.83	09:45:12.39	1.49	3x1200	2x2	RV31	+0.24 ± 0.02	193	1.90
F1-E1-F2009	10-25-2009	55129.43	06:40:39.86	09:43:59.35	1.17	3x1200	2x2	RV31	-0.18 ± 0.02	216	1.08
F1-E2-F2009	10-26-2009	55130.46	06:40:39.86	09:43:59.35	1.09	3x1200	2x2	RV31	+0.23 ± 0.02	216	1.93
F2-E1-F2009	10-25-2009	55129.48	06:40:48.66	09:35:52.50	1.08	3x1200	2x2	RV31	-0.08 ± 0.04	220	1.08
F2-E2-F2009	10-31-2009	55135.37	06:40:48.66	09:35:52.50	1.33	3x1200	2x2	RV31	+0.23 ± 0.03	220	0.88
F3-E1-F2009	10-31-2009	55135.42	06:40:54.85	09:41:10.59	1.13	3x1200	2x2	RV31	-0.02 ± 0.02	218	0.88
F3-E2-F2009	11-02-2009	55137.34	06:40:54.85	09:41:10.59	1.50	3x1200	2x2	RV31	-0.18 ± 0.08	218	0.97
F4-E1-F2009	10-31-2009	55135.48	06:40:41.37	09:46:36.31	1.08	3x1200	2x2	RV31	+0.14 ± 0.04	192	0.88
F4-E2-F2009	11-27-2009	55162.33	06:40:41.37	09:46:36.31	1.19	3x1200	2x2	RV31	+0.14 ± 0.04	208	0.79
F5-E1-F2009	11-02-2009	55137.40	06:40:50.32	09:35:29.87	1.20	3x1200	2x2	RV31	-0.02 ± 0.02	218	0.97
F5-E2-F2009	11-27-2009	55162.38	06:40:50.32	09:35:29.87	1.09	3x1200	2x2	RV31	-0.18 ± 0.08	218	0.79
F1-E1-S2010	01-31-2010	55227.28	06:40:42.70	09:44:11.34	1.14	3x1200	2x2	RV31	-0.07 ± 0.08	193	1.09
F1-E2-S2010	02-02-2010	55229.10	06:40:42.70	09:44:11.34	1.44	3x1200	2x2	RV31	0.03 ± 0.1	193	1.53
F2-E1-S2010	02-06-2010	55233.31	06:40:45.82	09:34:58.50	1.32	3x1200	2x2	RV31	0.01 ± 0.1	213	1.48
F2-E2-S2010	03-03-2010	55258.25	06:40:45.82	09:34:58.50	1.34	3x1200	2x2	RV31	0.19 ± 0.07	213	0.60
F3-E1-S2010	03-05-2010	55260.19	06:41:06.61	09:37:16.59	1.15	3x1200	2x2	RV31	0.20 ± 0.03	215	1.93
F3-E2-S2010	03-06-2010	55262.28	06:41:06.61	09:37:16.59	1.82	3x1200	2x2	RV31	0.12 ± 0.04	212	1.33
F4-E1-S2010	03-31-2010	55262.28	06:40:41.37	09:46:48.31	1.13	3x1200	2x2	RV31	0.05 ± 0.04	209	1.52
F4-E2-S2010	04-03-2010	55262.28	06:40:41.37	09:46:48.31	1.15	4x1200	2x2	RV31	-0.1 ± 0.04	209	1.63

<sup>a</sup>Shift applied is relative to the velocities in Fűrész et al. (2006).

Table 2. MIKE Fibers Observations

Field ID	Start Date UT Date	Julian Date (2400000)	RA (J2000)	Dec. (J2000)	Airmass	Exposure Time # × seconds	Binning	Filter	Zeropoint Shift km s <sup>-1</sup>	Number of Targets
A-1	12-10-2009	55175.81	06:41:00.98	09:32:44.4	1.4	3x1200	2x2	Mg	0.05± 0.1	220
B-1	12-11-2009	55179.81	06:40:48.90	09:51:44.4	1.4	3x1200	2x2	Mg	-0.13 ± 0.05	215
A-2	12-14-2009	55176.80	06:41:00.98	09:32:44.4	1.4	3x1200	2x2	Mg	0.31± 0.05	220
B-2	12-15-2009	55180.83	06:40:48.90	09:51:44.4	1.5	3x900	2x2	Mg	0.08 ± 0.04	215

<sup>a</sup>Shift applied is relative to the velocities in Fűrész et al. (2006).

Note. —

Table 3. Velocity Summary

2massID	RA (J2000)	Dec. (J2000)	$\overline{RV}^a$ (km s <sup>-1</sup> )	N Epochs <sup>b</sup>	Lithium EW (Å)	Spectral Type	K - [3.6]	[3.6] - [4.5]
0639037+094023	06:39: 3.75	09:40:23.4	5.32 ± 0.13	4	-99.00	-99.0	-99.00	-99.00
0639152+093937	06:39:15.25	09:39:37.8	29.88 ± 0.24	7	-99.00	-99.0	-99.00	-99.00
0639153+095303	06:39:15.37	09:53:03.6	102.33 ± 0.95	3	-99.00	-99.0	-99.00	-99.00
0639155+092444	06:39:15.55	09:24:44.8	10.94 ± 0.07	2	-99.00	-99.0	-99.00	-99.00
0639156+093912	06:39:15.63	09:39:13.0	1.43 ± 0.42	9	-99.00	-99.0	-99.00	-99.00
0639157+092929	06:39:15.70	09:29:29.4	18.65 ± 0.02	3	-99.00	-99.0	-99.00	-99.00
0639163+091953	06:39:16.37	09:19:53.3	50.59 ± 0.05	3	-99.00	-99.0	-99.00	-99.00
0639164+093116	06:39:16.45	09:31:16.1	1.63 ± 0.11	2	-99.00	-99.0	-99.00	-99.00
0639166+100055	06:39:16.62	10:00:55.3	-15.80 ± 0.06	2	-99.00	-99.0	-99.00	-99.00
0639168+091741	06:39:16.85	09:17:41.0	41.96 ± 0.12	2	-99.00	-99.0	-99.00	-99.00
0639172+093052	06:39:17.25	09:30:52.9	2.87 ± 0.17	2	-99.00	-99.0	-99.00	-99.00
0639174+092137	06:39:17.43	09:21:37.8	23.83 ± 0.27	5	-99.00	-99.0	-99.00	-99.00
0639174+092537	06:39:17.43	09:25:37.9	15.92 ± 0.16	2	-99.00	-99.0	-99.00	-99.00
0639175+095314	06:39:17.50	09:53:14.8	1.47 ± 0.42	2	-99.00	-99.0	-99.00	-99.00
0639176+093326	06:39:17.68	09:33:26.4	67.09 ± 0.20	2	-99.00	-99.0	-99.00	-99.00
0639179+091822	06:39:17.97	09:18:22.6	39.78 ± 0.01	2	-99.00	-99.0	-99.00	-99.00
0639180+092957	06:39:18.06	09:29:57.5	80.57 ± 0.28	2	-99.00	-99.0	-99.00	-99.00
0639180+094115	06:39:18.02	09:41:15.4	46.02 ± 0.31	2	-99.00	-99.0	-99.00	-99.00
0639185+094250	06:39:18.54	09:42:50.4	48.01 ± 0.30	2	-99.00	-99.0	-99.00	-99.00
0639186+094752	06:39:18.67	09:47:52.3	128.27 ± 4.50	2	-99.00	-99.0	-99.00	-99.00
0639189+093105	06:39:18.98	09:31:05.5	21.90 ± 0.09	2	-99.00	-99.0	-99.00	-99.00
0639189+094222	06:39:18.97	09:42:22.9	26.30 ± 0.20	2	-99.00	-99.0	-99.00	-99.00
0639190+092100	06:39:19.09	09:21:00.0	31.14 ± 0.17	2	-99.00	-99.0	-99.00	-99.00
0639191+092743	06:39:19.19	09:27:43.6	50.19 ± 0.37	2	-99.00	-99.0	-99.00	-99.00
0639192+095135	06:39:19.21	09:51:35.6	20.82 ± 0.01	2	-99.00	-99.0	-99.00	-99.00
0639196+092856	06:39:19.60	09:28:56.0	53.08 ± 0.05	2	-99.00	-99.0	-99.00	-99.00
0639196+093111	06:39:19.60	09:31:11.8	1.17 ± 0.39	2	-99.00	-99.0	-99.00	-99.00
0639197+092650	06:39:19.70	09:26:50.2	34.87 ± 0.01	2	-99.00	-99.0	-99.00	-99.00
0639201+095014	06:39:20.15	09:50:14.5	79.71 ± 0.01	2	-99.00	-99.0	-99.00	-99.00
0639201+095034	06:39:20.13	09:50:34.9	65.94 ± 0.72	2	-99.00	-99.0	-99.00	-99.00
0639206+095856	06:39:20.66	09:58:56.4	-1.20 ± 0.39	2	-99.00	-99.0	-99.00	-99.00
0639211+093627	06:39:21.11	09:36:27.9	0.09 ± 0.34	2	-99.00	-99.0	-99.00	-99.00
0639214+095949	06:39:21.42	09:59:49.4	-14.85 ± 0.06	2	-99.00	-99.0	-99.00	-99.00
0639216+094507	06:39:21.62	09:45:07.6	22.26 ± 2.10	2	-99.00	-99.0	-99.00	-99.00
0639217+095423	06:39:21.71	09:54:23.2	51.59 ± 0.14	2	-99.00	-99.0	-99.00	-99.00
0639218+095559	06:39:21.88	09:55:59.3	20.01 ± 0.05	2	-99.00	-99.0	-99.00	-99.00
0639220+093523	06:39:22.02	09:35:23.7	77.90 ± 0.14	2	-99.00	-99.0	-99.00	-99.00
0639223+094321	06:39:22.33	09:43:21.6	53.24 ± 0.48	2	-99.00	-99.0	-99.00	-99.00
0639224+094510	06:39:22.44	09:45:10.6	23.42 ± 0.95	2	-99.00	-99.0	-99.00	-99.00
0639226+093038	06:39:22.60	09:30:38.0	43.78 ± 0.46	3	-99.00	-99.0	-99.00	-99.00
0639226+095430	06:39:22.69	09:54:30.7	4.30 ± 0.88	7	-99.00	-99.0	-99.00	-99.00
0639229+093523	06:39:22.93	09:35:23.4	-27.28 ± 0.19	6	-99.00	-99.0	-99.00	-99.00
0639229+093616	06:39:22.94	09:36:16.9	-0.68 ± 0.09	7	-99.00	-99.0	-99.00	-99.00
0639232+094008	06:39:23.26	09:40:08.7	5.61 ± 0.04	2	-99.00	-99.0	-99.00	-99.00

Table 3—Continued

2massID	RA (J2000)	Dec. (J2000)	$\overline{RV}^a$ (km s <sup>-1</sup> )	N Epochs <sup>b</sup>	Lithium EW (Å)	Spectral Type	K - [3.6]	[3.6] - [4.5]
0639232+094703	06:39:23.20	09:47:03.6	29.55 ± 0.08	2	-99.00	-99.0	-99.00	-99.00
0639235+092055	06:39:23.56	09:20:55.0	60.13 ± 0.75	2	-99.00	-99.0	-99.00	-99.00
0639239+094201	06:39:23.97	09:42:01.7	66.55 ± 0.18	5	-99.00	-99.0	-99.00	-99.00
0639240+092550	06:39:24.01	09:25:50.8	28.97 ± 0.20	4	-99.00	-99.0	-99.00	-99.00
0639240+095231	06:39:24.05	09:52:31.4	98.19 ± 0.65	2	-99.00	-99.0	-99.00	-99.00
0639241+091805	06:39:24.15	09:18:05.8	-34.26 ± 0.16	4	-99.00	-99.0	-99.00	-99.00
0639243+095619	06:39:24.32	09:56:19.3	-29.75 ± 0.32	6	-99.00	-99.0	-99.00	-99.00
0639244+094903	06:39:24.42	09:49:03.7	31.90 ± 1.06	2	-99.00	-99.0	-99.00	-99.00
0639245+095040	06:39:24.55	09:50:40.2	70.09 ± 0.11	5	-99.00	-99.0	-99.00	-99.00
0639246+091721	06:39:24.68	09:17:21.6	54.04 ± 0.31	3	-99.00	-99.0	-99.00	-99.00
0639246+092233	06:39:24.65	09:22:33.2	3.18 ± 0.10	7	-99.00	-99.0	-99.00	-99.00
0639249+092207	06:39:24.97	09:22:07.5	1.73 ± 1.10	2	-99.00	-99.0	-99.00	-99.00
0639253+092535	06:39:25.35	09:25:35.7	20.35 ± 0.03	2	-99.00	-99.0	-99.00	-99.00
0639253+094314	06:39:25.36	09:43:14.7	-22.56 ± 0.01	2	-99.00	-99.0	-99.00	-99.00
0639256+094253	06:39:25.64	09:42:53.6	2.50 ± 0.19	2	-99.00	-99.0	-99.00	-99.00
0639258+093812	06:39:25.81	09:38:12.4	1.76 ± 0.35	2	-99.00	-99.0	-99.00	-99.00
0639262+094110	06:39:26.26	09:41:10.8	0.72 ± 0.23	10	-99.00	-99.0	-99.00	-99.00
0639264+094329	06:39:26.49	09:43:29.8	-1.19 ± 0.77	2	-99.00	-99.0	-99.00	-99.00
0639266+093037	06:39:26.65	09:30:37.9	12.79 ± 0.03	2	-99.00	-99.0	-99.00	-99.00
0639268+091921	06:39:26.80	09:19:21.5	35.10 ± 0.18	2	-99.00	-99.0	-99.00	-99.00
0639269+094122	06:39:26.92	09:41:22.0	-7.88 ± 0.76	2	-99.00	-99.0	-99.00	-99.00
0639275+092309	06:39:27.58	09:23:09.2	19.15 ± 0.14	6	-99.00	-99.0	-99.00	-99.00
0639275+095100	06:39:27.59	09:51:00.9	72.49 ± 0.15	5	-99.00	-99.0	-99.00	-99.00
0639280+093556	06:39:28.05	09:35:56.2	72.99 ± 0.13	2	-99.00	-99.0	-99.00	-99.00
0639283+095358	06:39:28.35	09:53:59.0	-14.29 ± 0.14	4	-99.00	-99.0	-99.00	-99.00
0639287+092640	06:39:28.72	09:26:41.0	-21.70 ± 0.81	6	-99.00	-99.0	-99.00	-99.00
0639287+095459	06:39:28.73	09:54:59.9	-40.19 ± 0.17	2	-99.00	-99.0	-99.00	-99.00
0639293+092058	06:39:29.36	09:20:58.9	10.05 ± 0.21	6	-99.00	-99.0	-99.00	-99.00
0639293+094339	06:39:29.36	09:43:39.8	0.36 ± 0.26	2	-99.00	-99.0	-99.00	-99.00
0639295+094813	06:39:29.59	09:48:13.4	29.41 ± 0.37	2	-99.00	-99.0	-99.00	-99.00
0639303+092300	06:39:30.32	09:23:00.0	93.97 ± 0.11	4	-99.00	-99.0	-99.00	-99.00
0639303+093337	06:39:30.38	09:33:37.5	3.81 ± 0.56	8	-99.00	-99.0	-99.00	-99.00
0639304+094924	06:39:30.44	09:49:24.1	-24.37 ± 0.06	5	-99.00	-99.0	-99.00	-99.00
0639305+092850	06:39:30.54	09:28:50.1	45.90 ± 0.25	2	-99.00	-99.0	-99.00	-99.00
0639311+095330	06:39:31.14	09:53:30.5	-16.24 ± 0.24	4	-99.00	-99.0	-99.00	-99.00
0639314+093037	06:39:31.45	09:30:37.8	44.35 ± 0.48	2	-99.00	-99.0	-99.00	-99.00
0639316+094735	06:39:31.61	09:47:35.5	-16.71 ± 0.15	2	-99.00	-99.0	-99.00	-99.00
0639322+094953	06:39:32.27	09:49:53.0	65.38 ± 0.75	2	-99.00	-99.0	-99.00	-99.00
0639327+095103	06:39:32.78	09:51:03.9	36.54 ± 0.45	2	-99.00	-99.0	-99.00	-99.00
0639329+095629	06:39:32.98	09:56:29.4	8.88 ± 0.17	7	-99.00	-99.0	-99.00	-99.00
0639330+092720	06:39:33.01	09:27:20.6	75.45 ± 0.52	2	-99.00	-99.0	-99.00	-99.00
0639332+094842	06:39:33.27	09:48:42.3	29.28 ± 0.33	2	-99.00	-99.0	-99.00	-99.00
0639333+093011	06:39:33.33	09:30:11.8	47.11 ± 1.19	4	-99.00	-99.0	-99.00	-99.00
0639333+095201	06:39:33.40	09:52:01.7	2.87 ± 0.76	8	-99.00	-99.0	-99.00	-99.00

Table 3—Continued

2massID	RA (J2000)	Dec. (J2000)	$\overline{RV}^a$ (km s <sup>-1</sup> )	N Epochs <sup>b</sup>	Lithium EW (Å)	Spectral Type	K - [3.6]	[3.6] - [4.5]
0639334+094728	06:39:33.41	09:47:28.9	20.64 ± 0.09	2	-99.00	-99.0	-99.00	-99.00
0639335+095140	06:39:33.57	09:51:40.5	11.23 ± 0.36	9	-99.00	-99.0	-99.00	-99.00
0639337+093331	06:39:33.72	09:33:31.0	75.93 ± 1.68	2	-99.00	-99.0	-99.00	-99.00
0639339+092949	06:39:33.97	09:29:50.0	72.69 ± 1.00	2	-99.00	-99.0	-99.00	-99.00
0639339+094920	06:39:33.99	09:49:20.9	5.33 ± 0.26	9	-99.00	-99.0	-99.00	-99.00
0639342+094645	06:39:34.27	09:46:45.0	-1.03 ± 0.88	6	-99.00	-99.0	-99.00	-99.00
0639344+095451	06:39:34.41	09:54:51.3	4.77 ± 0.18	8	-99.00	-99.0	-99.00	-99.00
0639346+092440	06:39:34.67	09:24:40.2	37.20 ± 0.08	6	-99.00	-99.0	-99.00	-99.00
0639347+094654	06:39:34.75	09:46:54.2	-0.49 ± 0.75	9	-99.00	-99.0	-99.00	-99.00
0639349+093336	06:39:34.91	09:33:36.1	40.70 ± 1.69	3	-99.00	-99.0	-99.00	-99.00
0639353+093232	06:39:35.34	09:32:32.3	12.76 ± 0.44	7	-99.00	-99.0	-99.00	-99.00
0639360+092426	06:39:36.03	09:24:26.2	-1.21 ± 0.22	7	-99.00	-99.0	-99.00	-99.00
0639360+094045	06:39:36.05	09:40:45.3	-35.50 ± 0.48	5	-99.00	-99.0	-99.00	-99.00
0639363+095631	06:39:36.34	09:56:31.2	234.07 ± 0.48	2	-99.00	-99.0	-99.00	-99.00
0639365+094138	06:39:36.54	09:41:38.7	22.10 ± 0.02	2	-99.00	-99.0	-99.00	-99.00
0639373+092637	06:39:37.34	09:26:37.5	24.09 ± 0.16	3	-99.00	-99.0	-99.00	-99.00
0639375+093131	06:39:37.58	09:31:31.0	53.58 ± 0.05	2	-99.00	-99.0	-99.00	-99.00
0639381+095307	06:39:38.19	09:53:07.9	1.93 ± 1.39	2	-99.00	-99.0	-99.00	-99.00
0639382+092837	06:39:38.27	09:28:37.3	9.91 ± 2.67	4	-99.00	-99.0	-99.00	-99.00
0639386+094044	06:39:38.67	09:40:44.1	36.32 ± 0.72	2	-99.00	-99.0	-99.00	-99.00
0639388+095151	06:39:38.84	09:51:51.8	5.72 ± 0.41	8	-99.00	-99.0	-99.00	-99.00
0639396+094544	06:39:39.62	09:45:44.3	28.30 ± 0.08	5	-99.00	-99.0	-99.00	-99.00
0639397+094812	06:39:39.74	09:48:12.9	61.85 ± 0.04	2	-99.00	-99.0	-99.00	-99.00
0639402+091821	06:39:40.25	09:18:21.8	-0.75 ± 1.33	4	-99.00	-99.0	-99.00	-99.00
0639403+092607	06:39:40.32	09:26:07.4	-12.14 ± 0.16	4	-99.00	-99.0	-99.00	-99.00
0639414+094619	06:39:41.48	09:46:19.7	3.74 ± 0.44	10	-99.00	-99.0	-99.00	-99.00
0639415+093440	06:39:41.57	09:34:40.5	0.92 ± 0.11	6	-99.00	-99.0	-99.00	-99.00
0639417+094851	06:39:41.79	09:48:51.4	23.09 ± 0.69	2	-99.00	-99.0	-99.00	-99.00
0639418+091804	06:39:41.88	09:18:04.5	1.65 ± 0.68	2	-99.00	-99.0	-99.00	0.04
0639418+100029	06:39:41.81	10:00:29.9	47.50 ± 1.93	2	-99.00	-99.0	-99.00	-99.00
0639419+094719	06:39:41.97	09:47:19.7	35.44 ± 0.16	2	-99.00	-99.0	-99.00	-99.00
0639419+095132	06:39:41.92	09:51:32.3	21.89 ± 1.23	2	-99.00	-99.0	-99.00	-99.00
0639422+095631	06:39:42.24	09:56:31.1	118.91 ± 0.27	6	-99.00	-99.0	-99.00	-99.00
0639425+095513	06:39:42.53	09:55:13.3	8.74 ± 0.15	2	-99.00	-99.0	-99.00	-99.00
0639426+093151	06:39:42.65	09:31:51.4	11.20 ± 0.10	3	-99.00	-99.0	-99.00	-99.00
0639426+095534	06:39:42.66	09:55:34.5	8.26 ± 0.10	2	-99.00	-99.0	-99.00	-99.00
0639430+092601	06:39:43.07	09:26:01.7	-0.31 ± 0.96	8	-99.00	-99.0	-99.00	-99.00
0639432+092519	06:39:43.26	09:25:19.5	79.47 ± 1.59	3	-99.00	-99.0	-99.00	-99.00
0639433+093854	06:39:43.35	09:38:54.3	3.48 ± 0.57	2	-99.00	-99.0	-99.00	-99.00
0639436+095745	06:39:43.65	09:57:45.7	-18.96 ± 0.09	2	-99.00	-99.0	0.29	0.01
0639441+095403	06:39:44.16	09:54:03.7	3.63 ± 0.32	2	-99.00	-99.0	0.14	-0.06
0639441+095704	06:39:44.19	09:57:04.3	42.39 ± 0.32	2	-99.00	-99.0	0.30	-0.17
0639443+100055	06:39:44.37	10:00:55.2	67.86 ± 0.15	5	-99.00	-99.0	21.12	-20.97
0639451+094642	06:39:45.18	09:46:43.0	-84.91 ± 0.13	5	-99.00	-99.0	0.06	0.01



Table 3—Continued

2massID	RA (J2000)	Dec. (J2000)	$\overline{RV}^a$ (km s <sup>-1</sup> )	N Epochs <sup>b</sup>	Lithium EW (Å)	Spectral Type	K - [3.6]	[3.6] - [4.5]
0639454+092439	06:39:45.44	09:24:39.7	12.34 ± 0.17	3	-99.00	-99.0	0.34	0.04
0639460+095724	06:39:46.00	09:57:24.6	-24.50 ± 0.22	4	-99.00	-99.0	0.26	-0.01
0639461+095803	06:39:46.12	09:58:03.3	-30.73 ± 0.23	4	-99.00	-99.0	0.02	-0.01
0639462+094819	06:39:46.27	09:48:19.8	-0.12 ± 0.33	10	-99.00	-99.0	0.20	-0.03
0639472+092418	06:39:47.24	09:24:18.1	-29.16 ± 2.11	2	-99.00	-99.0	-0.16	0.02
0639477+092606	06:39:47.72	09:26:06.7	12.57 ± 0.29	7	-99.00	-99.0	0.02	0.02
0639481+095905	06:39:48.20	09:59:05.7	12.14 ± 0.30	6	-99.00	-99.0	0.15	-0.06
0639483+094852	06:39:48.36	09:48:52.6	-11.61 ± 0.09	4	-99.00	-99.0	-0.02	0.04
0639488+094306	06:39:48.89	09:43:06.2	34.72 ± 0.07	4	-99.00	-99.0	0.05	0.02
0639496+093322	06:39:49.60	09:33:22.1	0.11 ± 0.17	6	-99.00	-99.0	0.13	0.02
0639497+095838	06:39:49.74	09:58:38.8	41.25 ± 0.36	2	-99.00	-99.0	-99.00	0.03
0639498+095621	06:39:49.83	09:56:21.8	10.61 ± 0.35	10	-99.00	-99.0	0.27	-0.03
0639502+095817	06:39:50.22	09:58:17.2	69.27 ± 0.09	2	-99.00	-99.0	-99.00	-0.07
0639510+093632	06:39:51.10	09:36:32.8	5.38 ± 4.26	3	-99.00	-99.0	0.09	0.06
0639523+091909	06:39:52.33	09:19:09.5	13.67 ± 0.15	8	-99.00	-99.0	0.23	0.00
0639526+095831	06:39:52.65	09:58:31.1	27.21 ± 0.09	2	-99.00	-99.0	-99.00	0.04
0639527+095830	06:39:52.72	09:58:30.8	27.08 ± 0.84	2	-99.00	-99.0	-99.00	0.04
0639528+092807	06:39:52.87	09:28:07.5	1.85 ± 0.16	3	-99.00	-99.0	0.00	0.02
0639532+094945	06:39:53.28	09:49:45.8	2.57 ± 2.38	2	-99.00	-99.0	-99.00	-0.03
0639552+095911	06:39:55.29	09:59:11.3	-29.88 ± 0.17	2	-99.00	-99.0	-99.00	0.03
0639557+093428	06:39:55.76	09:34:28.5	45.48 ± 0.16	4	-99.00	-99.0	0.11	-0.03
0639560+095850	06:39:56.06	09:58:50.1	38.12 ± 0.01	2	-99.00	-99.0	-99.00	-0.05
0639561+093046	06:39:56.18	09:30:46.2	7.23 ± 0.23	9	-99.00	-99.0	0.03	0.04
0639563+094331	06:39:56.39	09:43:31.5	18.61 ± 0.09	4	-99.00	-99.0	-0.01	0.01
0639568+094425	06:39:56.83	09:44:25.2	5.59 ± 0.06	7	-99.00	-99.0	0.19	0.00
0639571+091728	06:39:57.19	09:17:28.9	-22.92 ± 0.01	2	-99.00	-99.0	0.04	-0.02
0639576+092323	06:39:57.65	09:23:23.2	8.86 ± 2.11	3	-99.00	-99.0	0.15	-0.01
0639588+095845	06:39:58.80	09:58:45.5	20.92 ± 0.28	2	-99.00	-99.0	0.21	-0.07
0639592+092724	06:39:59.24	09:27:24.5	5.70 ± 0.64	7	-99.00	-99.0	0.36	0.11
0640009+092044	06:40: 0.90	09:20:44.4	28.64 ± 0.29	2	-99.00	-99.0	-99.00	0.02
0640011+093533	06:40: 1.12	09:35:33.5	1.65 ± 0.40	8	0.60	70.5	0.15	0.06
0640012+094236	06:40: 1.22	09:42:36.5	-1.32 ± 0.45	2	-99.00	-99.0	0.14	0.04
0640012+094642	06:40: 1.26	09:46:42.5	-54.75 ± 0.08	2	-99.00	-99.0	0.22	-0.01
0640014+093105	06:40: 1.44	09:31:05.8	2.73 ± 0.25	10	-99.00	-99.0	0.15	-0.03
0640026+093524	06:40: 2.67	09:35:24.3	0.39 ± 1.13	8	0.36	70.7	0.46	0.28
0640031+095008	06:40: 3.15	09:50:08.6	72.96 ± 0.28	6	-99.00	-99.0	0.17	-0.05
0640032+095835	06:40: 3.22	09:58:35.8	36.04 ± 3.48	2	-99.00	-99.0	0.34	0.04
0640038+095812	06:40: 3.85	09:58:12.2	11.10 ± 0.24	2	0.00	66.0	-99.00	-0.01
0640051+093350	06:40: 5.11	09:33:50.3	-50.98 ± 0.21	5	-99.00	-99.0	0.02	0.04
0640051+094618	06:40: 5.17	09:46:18.1	4.06 ± 0.81	7	-99.00	-99.0	0.17	-0.01
0640055+092226	06:40: 5.53	09:22:26.1	0.57 ± 1.11	3	-99.00	-99.0	-21.16	0.26
0640056+093549	06:40: 5.66	09:35:49.3	1.94 ± 0.21	4	-99.00	-99.0	0.03	0.04
0640059+095750	06:40: 5.99	09:57:51.0	2.80 ± 0.29	6	0.66	64.0	0.15	0.04
0640060+094942	06:40: 6.01	09:49:42.7	7.44 ± 0.45	9	-99.00	-99.0	0.43	0.30

Table 3—Continued

2massID	RA (J2000)	Dec. (J2000)	$\overline{RV}^a$ (km s <sup>-1</sup> )	N Epochs <sup>b</sup>	Lithium EW (Å)	Spectral Type	K - [3.6]	[3.6] - [4.5]
0640063+093933	06:40: 6.38	09:39:33.6	0.23 ± 0.22	7	-99.00	-99.0	0.09	-0.02
0640066+092033	06:40: 6.66	09:20:33.3	-1.00 ± 0.11	2	-99.00	-99.0	0.03	-0.01
0640075+095653	06:40: 7.59	09:56:53.3	3.67 ± 0.60	2	0.32	70.0	0.28	0.03
0640076+094446	06:40: 7.69	09:44:46.6	87.69 ± 0.06	3	-99.00	-99.0	0.18	-0.02
0640083+095726	06:40: 8.35	09:57:26.2	-31.99 ± 0.08	2	-99.00	-99.0	0.16	0.03
0640084+095926	06:40: 8.43	09:59:26.0	-1.33 ± 1.40	2	0.76	71.2	-99.00	0.00
0640086+095513	06:40: 8.63	09:55:13.9	37.91 ± 0.13	2	-99.00	-99.0	0.20	0.09
0640088+091909	06:40: 8.83	09:19:09.1	-22.14 ± 0.75	6	-99.00	-99.0	0.11	0.14
0640091+092058	06:40: 9.17	09:20:58.1	43.52 ± 0.55	2	-99.00	-99.0	-99.00	-0.02
0640102+095009	06:40:10.28	09:50:09.5	-78.02 ± 2.59	2	-99.00	-99.0	0.33	0.07
0640103+093442	06:40:10.35	09:34:43.0	108.93 ± 0.67	2	-99.00	-99.0	0.32	0.14
0640105+091726	06:40:10.59	09:17:26.9	62.83 ± 1.70	2	-99.00	-99.0	-99.00	0.03
0640108+094007	06:40:10.89	09:40:07.3	-0.11 ± 0.97	7	-99.00	-99.0	0.17	0.08
0640111+093805	06:40:11.13	09:38:05.9	6.86 ± 0.41	9	-99.00	-99.0	0.74	0.32
0640114+094142	06:40:11.40	09:41:42.8	28.54 ± 0.10	5	-99.00	-99.0	0.13	-0.02
0640115+095922	06:40:11.55	09:59:22.9	53.26 ± 0.41	2	-99.00	-99.0	-99.00	-0.02
0640120+101145	06:40:12.00	10:11:45.7	1.76 ± 1.95	2	-99.00	-99.0	-99.00	-99.00
0640124+092813	06:40:12.50	09:28:13.1	-13.75 ± 0.22	5	-99.00	-99.0	0.06	-0.06
0640124+094423	06:40:12.44	09:44:23.1	4.24 ± 0.81	7	-99.00	-99.0	0.20	0.03
0640125+100540	06:40:12.58	10:05:40.5	7.34 ± 0.31	5	-99.00	-99.0	-99.00	0.23
0640127+095903	06:40:12.76	09:59:03.3	39.42 ± 0.08	2	-99.00	-99.0	-99.00	-0.02
0640130+092103	06:40:13.10	09:21:03.5	9.65 ± 0.49	2	-99.00	-99.0	0.12	-0.06
0640134+091927	06:40:13.45	09:19:27.6	-6.26 ± 0.26	4	-99.00	-99.0	0.09	-0.05
0640137+095206	06:40:13.77	09:52:06.7	11.52 ± 0.05	2	-99.00	-99.0	0.05	-0.06
0640137+095630	06:40:13.70	09:56:30.6	8.12 ± 0.99	3	-99.00	-99.0	0.98	0.62
0640142+094652	06:40:14.23	09:46:52.8	-31.85 ± 0.40	7	-99.00	-99.0	0.07	-0.02
0640151+100157	06:40:15.16	10:01:57.8	3.97 ± 0.63	3	-99.00	-99.0	-99.00	0.36
0640153+094242	06:40:15.35	09:42:42.4	12.08 ± 0.42	8	0.38	65.9	0.14	-0.06
0640153+095918	06:40:15.39	09:59:18.6	-28.12 ± 2.59	2	-99.00	-99.0	0.12	0.07
0640155+092534	06:40:15.58	09:25:34.5	-42.95 ± 0.29	4	-99.00	-99.0	0.15	-0.10
0640160+095737	06:40:16.04	09:57:37.7	-5.04 ± 0.48	3	0.00	61.0	0.24	0.00
0640166+094022	06:40:16.69	09:40:22.6	10.38 ± 1.26	2	-99.00	-99.0	0.43	0.14
0640176+094758	06:40:17.62	09:47:58.0	0.54 ± 0.94	2	0.00	65.7	0.19	0.05
0640180+095022	06:40:18.02	09:50:22.1	3.90 ± 2.91	2	-99.00	-99.0	0.28	0.10
0640186+100024	06:40:18.64	10:00:24.8	3.47 ± 0.67	4	-99.00	-99.0	1.19	0.61
0640199+095738	06:40:19.94	09:57:38.4	45.07 ± 0.17	3	-99.00	-99.0	0.13	0.01
0640200+092828	06:40:20.09	09:28:28.5	5.56 ± 0.04	2	0.67	67.0	0.33	0.34
0640202+095606	06:40:20.27	09:56:06.4	8.14 ± 1.65	7	-99.00	-99.0	0.60	0.39
0640209+092354	06:40:20.96	09:23:54.2	-11.87 ± 0.12	3	-99.00	-99.0	0.19	-0.03
0640210+094628	06:40:21.06	09:46:28.0	6.96 ± 0.94	2	0.00	66.0	0.20	0.04
0640211+095902	06:40:21.16	09:59:02.5	15.27 ± 0.69	10	0.19	65.9	0.21	0.14
0640213+092014	06:40:21.31	09:20:14.2	-19.13 ± 0.22	4	-99.00	-99.0	0.03	-0.01
0640222+095428	06:40:22.22	09:54:28.9	6.57 ± 0.35	6	-99.00	-99.0	0.17	0.00
0640231+095619	06:40:23.13	09:56:19.9	-45.05 ± 0.79	2	-99.00	-99.0	0.05	-0.06

Table 3—Continued

2massID	RA (J2000)	Dec. (J2000)	$\overline{RV}^a$ (km s <sup>-1</sup> )	N Epochs <sup>b</sup>	Lithium EW (Å)	Spectral Type	K - [3.6]	[3.6] - [4.5]
0640234+095455	06:40:23.42	09:54:55.6	7.74 ± 1.60	4	-99.00	-99.0	0.70	0.27
0640234+095923	06:40:23.48	09:59:23.3	22.30 ± 0.10	3	-99.00	-99.0	0.22	-0.06
0640234+100135	06:40:23.46	10:01:35.7	6.98 ± 4.96	2	0.00	71.9	-99.00	0.12
0640236+095951	06:40:23.69	09:59:51.5	29.38 ± 0.14	7	-99.00	-99.0	0.15	-0.05
0640237+095523	06:40:23.73	09:55:23.9	8.18 ± 0.90	10	-99.00	-99.0	0.72	0.42
0640241+093412	06:40:24.16	09:34:12.5	2.03 ± 0.57	2	0.56	68.7	0.77	0.48
0640254+094825	06:40:25.48	09:48:26.0	9.47 ± 0.28	5	-99.00	-99.0	0.09	0.02
0640256+095835	06:40:25.69	09:58:35.6	5.31 ± 0.12	4	-99.00	-99.0	0.07	-0.01
0640256+095959	06:40:25.65	09:59:59.7	4.36 ± 0.71	5	-99.00	-99.0	0.54	0.28
0640257+100111	06:40:25.73	10:01:11.2	-31.08 ± 0.09	2	-99.00	-99.0	0.15	0.03
0640260+095820	06:40:26.08	09:58:20.8	14.63 ± 2.63	2	-99.00	-99.0	-99.00	0.01
0640265+093522	06:40:26.52	09:35:22.0	4.98 ± 2.66	2	0.60	68.9	0.22	0.05
0640267+092528	06:40:26.76	09:25:28.3	35.07 ± 0.52	4	-99.00	-99.0	0.01	-0.08
0640272+092036	06:40:27.29	09:20:36.9	-67.59 ± 0.63	2	-99.00	-99.0	0.22	-0.04
0640272+092221	06:40:27.22	09:22:21.2	-9.24 ± 0.11	2	-99.00	-99.0	0.12	0.13
0640273+092727	06:40:27.38	09:27:27.5	-107.35 ± 0.68	2	-99.00	-99.0	0.28	0.18
0640281+092345	06:40:28.15	09:23:45.6	3.27 ± 1.29	2	-99.00	-99.0	0.21	0.05
0640284+095831	06:40:28.49	09:58:31.9	60.10 ± 0.06	2	-99.00	-99.0	0.13	-0.01
0640285+093547	06:40:28.59	09:35:47.6	2.29 ± 0.29	9	0.57	68.0	0.10	-0.01
0640287+093100	06:40:28.78	09:31:00.3	1.30 ± 0.27	8	-99.00	-99.0	-20.01	0.02
0640289+094217	06:40:28.95	09:42:17.1	5.79 ± 0.23	8	0.58	67.4	0.28	-0.01
0640292+094407	06:40:29.25	09:44:07.5	4.32 ± 1.38	7	0.30	70.0	0.23	0.02
0640294+100047	06:40:29.47	10:00:47.8	-64.56 ± 0.26	5	-99.00	-99.0	0.11	0.01
0640296+091851	06:40:29.69	09:18:51.8	1.75 ± 0.41	2	-99.00	-99.0	0.15	0.06
0640297+095933	06:40:29.75	09:59:33.3	6.70 ± 0.33	12	-99.00	-99.0	0.14	-0.04
0640298+095010	06:40:29.89	09:50:10.4	9.87 ± 0.36	11	-99.00	-99.0	0.10	-0.04
0640305+095014	06:40:30.60	09:50:14.8	8.33 ± 1.51	6	1.02	70.4	0.63	0.28
0640306+094610	06:40:30.62	09:46:10.6	4.52 ± 0.39	12	-99.00	-99.0	0.08	0.00
0640307+094807	06:40:30.77	09:48:07.7	7.58 ± 0.74	7	-99.00	-99.0	0.08	0.22
0640309+100625	06:40:30.98	10:06:25.5	5.02 ± 0.29	2	-99.00	-99.0	-99.00	0.24
0640312+093107	06:40:31.27	09:31:07.5	-3.26 ± 1.14	2	-99.00	-99.0	-0.27	-0.02
0640313+094129	06:40:31.34	09:41:29.2	16.88 ± 0.40	9	-99.00	-99.0	0.21	0.04
0640316+094823	06:40:31.64	09:48:23.4	3.45 ± 0.36	8	-99.00	-99.0	0.20	0.04
0640318+093600	06:40:31.83	09:36:00.6	1.23 ± 0.21	2	0.62	70.5	0.17	0.02
0640318+094315	06:40:31.84	09:43:15.3	32.49 ± 2.87	2	-99.00	-99.0	0.10	0.08
0640328+095129	06:40:32.80	09:51:29.3	6.68 ± 0.98	7	-99.00	-99.0	0.16	0.04
0640329+093618	06:40:32.99	09:36:18.5	-103.16 ± 0.90	2	-99.00	-99.0	0.54	0.13
0640330+092311	06:40:33.00	09:23:11.1	34.84 ± 0.25	2	-99.00	-99.0	0.15	0.08
0640333+095853	06:40:33.33	09:58:53.0	5.18 ± 0.40	3	-99.00	-99.0	0.18	0.04
0640337+091718	06:40:33.73	09:17:18.9	22.58 ± 3.15	2	-99.00	-99.0	-0.20	0.02
0640337+093257	06:40:33.76	09:32:57.0	-45.70 ± 0.17	5	-99.00	-99.0	0.03	0.01
0640337+100019	06:40:33.73	10:00:19.3	40.91 ± 0.68	3	-99.00	-99.0	0.11	0.07
0640338+100250	06:40:33.84	10:02:50.4	22.61 ± 0.02	2	-99.00	-99.0	0.19	0.01
0640343+093851	06:40:34.30	09:38:51.7	-7.30 ± 0.17	8	-99.00	-99.0	0.02	-0.07

Table 3—Continued

2massID	RA (J2000)	Dec. (J2000)	$\overline{RV}^a$ (km s <sup>-1</sup> )	N Epochs <sup>b</sup>	Lithium EW (Å)	Spectral Type	K - [3.6]	[3.6] - [4.5]
0640344+093518	06:40:34.47	09:35:18.3	1.31 ± 0.43	8	-99.00	-99.0	0.49	0.16
0640347+095946	06:40:34.72	09:59:46.7	4.00 ± 0.56	3	-99.00	-99.0	0.19	0.00
0640347+100120	06:40:34.77	10:01:20.6	32.23 ± 0.21	3	-99.00	-99.0	0.14	0.00
0640363+092244	06:40:36.36	09:22:44.5	11.34 ± 0.26	8	-99.00	-99.0	0.15	0.04
0640365+095045	06:40:36.52	09:50:45.6	9.40 ± 0.69	10	0.63	68.8	0.73	0.35
0640366+094822	06:40:36.63	09:48:23.0	5.39 ± 0.28	10	-99.00	-99.0	0.14	-0.06
0640366+095203	06:40:36.66	09:52:03.2	4.91 ± 0.69	9	0.43	66.3	1.08	0.62
0640369+093909	06:40:36.98	09:39:09.8	8.43 ± 0.48	2	0.59	68.5	0.10	0.09
0640371+092651	06:40:37.20	09:26:51.3	-32.84 ± 0.23	5	-99.00	-99.0	0.01	-0.07
0640372+093109	06:40:37.21	09:31:09.9	5.13 ± 0.70	9	-99.00	-99.0	0.18	0.05
0640374+095521	06:40:37.46	09:55:21.3	4.73 ± 2.24	2	0.59	67.4	0.15	0.02
0640378+091730	06:40:37.85	09:17:30.2	-48.37 ± 0.05	2	-99.00	-99.0	-99.00	0.00
0640378+093454	06:40:37.87	09:34:54.0	1.30 ± 0.57	12	0.78	69.0	0.88	0.23
0640378+094010	06:40:37.80	09:40:10.6	10.73 ± 1.77	2	0.00	65.8	0.17	0.09
0640379+091816	06:40:37.91	09:18:16.7	-0.74 ± 0.01	2	-99.00	-99.0	-99.00	-0.03
0640380+093249	06:40:38.03	09:32:49.2	8.38 ± 6.07	2	-99.00	-99.0	0.20	-0.05
0640381+092952	06:40:38.20	09:29:52.5	1.35 ± 0.76	9	0.47	69.2	0.45	0.28
0640386+093656	06:40:38.68	09:36:57.0	4.21 ± 1.86	7	0.64	70.8	0.25	0.04
0640387+092138	06:40:38.78	09:21:38.3	4.42 ± 0.11	9	-99.00	-99.0	-0.05	0.01
0640390+093600	06:40:39.02	09:36:00.0	3.58 ± 0.24	2	0.58	68.0	0.25	0.07
0640391+095058	06:40:39.12	09:50:58.6	6.01 ± 0.25	7	-99.00	-99.0	0.90	0.44
0640393+093445	06:40:39.34	09:34:45.6	4.63 ± 1.13	8	-99.00	-99.0	2.06	0.73
0640394+094256	06:40:39.47	09:42:56.3	-20.04 ± 0.66	2	-99.00	-99.0	0.25	0.00
0640394+094839	06:40:39.48	09:48:40.0	85.01 ± 0.15	6	-99.00	-99.0	0.10	-0.07
0640395+091751	06:40:39.53	09:17:51.3	0.11 ± 0.21	2	-99.00	-99.0	0.23	0.00
0640400+093502	06:40:40.06	09:35:02.9	1.85 ± 0.19	7	-99.00	-99.0	1.07	0.27
0640400+095104	06:40:40.01	09:51:04.7	-29.58 ± 1.85	2	-99.00	-99.0	-99.00	0.04
0640402+100023	06:40:40.23	10:00:23.7	38.16 ± 2.19	3	-99.00	-99.0	0.11	0.00
0640410+092754	06:40:41.01	09:27:54.3	3.59 ± 0.49	10	0.59	67.6	0.33	0.09
0640410+094757	06:40:41.03	09:47:57.7	5.85 ± 0.20	9	0.64	67.0	0.20	-0.03
0640411+095256	06:40:41.14	09:52:56.5	4.35 ± 0.34	9	-99.00	-99.0	1.09	0.46
0640412+091757	06:40:41.28	09:17:57.0	3.08 ± 0.41	2	-99.00	-99.0	0.22	-0.06
0640412+095430	06:40:41.25	09:54:30.9	42.50 ± 0.95	2	-99.00	-99.0	0.31	0.01
0640413+095102	06:40:41.32	09:51:02.4	9.88 ± 0.57	7	0.46	68.2	0.81	0.35
0640413+095413	06:40:41.36	09:54:13.9	10.85 ± 0.35	11	-99.00	-99.0	0.77	0.36
0640414+094809	06:40:41.42	09:48:09.6	5.10 ± 0.44	7	-99.00	-99.0	0.04	0.05
0640415+095517	06:40:41.56	09:55:17.4	-29.72 ± 0.72	7	-99.00	-99.0	0.00	-0.01
0640419+094355	06:40:41.93	09:43:55.2	1.10 ± 1.27	7	0.69	70.8	0.68	0.22
0640424+093220	06:40:42.45	09:32:20.6	2.91 ± 0.30	11	0.42	66.0	0.13	-0.02
0640424+100153	06:40:42.40	10:01:53.5	32.92 ± 0.56	2	-99.00	-99.0	-0.09	0.12
0640426+095348	06:40:42.62	09:53:48.0	9.35 ± 0.55	2	-99.00	-99.0	-21.62	0.02
0640432+093114	06:40:43.24	09:31:15.0	1.66 ± 0.70	7	0.50	71.2	0.27	0.10
0640433+095059	06:40:43.35	09:50:59.5	6.53 ± 0.30	8	-99.00	-99.0	0.11	0.02
0640434+092840	06:40:43.43	09:28:40.9	1.67 ± 0.22	8	0.58	68.7	0.09	0.10

Table 3—Continued

2massID	RA (J2000)	Dec. (J2000)	$\overline{RV}^a$ (km s <sup>-1</sup> )	N Epochs <sup>b</sup>	Lithium EW (Å)	Spectral Type	K - [3.6]	[3.6] - [4.5]
0640436+091704	06:40:43.60	09:17:04.0	46.40 ± 0.12	2	-99.00	-99.0	0.16	0.02
0640441+092355	06:40:44.13	09:23:55.4	-2.20 ± 0.50	8	-99.00	-99.0	0.00	-0.01
0640442+095339	06:40:44.24	09:53:39.4	5.74 ± 3.28	2	0.00	72.3	0.31	0.22
0640445+093226	06:40:44.59	09:32:26.2	-3.16 ± 0.28	2	-99.00	-99.0	0.42	0.15
0640445+094812	06:40:44.59	09:48:12.6	6.21 ± 0.40	2	-99.00	-99.0	-20.50	0.05
0640451+092844	06:40:45.16	09:28:44.4	1.20 ± 0.55	7	-99.00	-99.0	0.50	0.17
0640452+092354	06:40:45.21	09:23:54.7	12.32 ± 3.27	6	-99.00	-99.0	0.09	0.10
0640455+095123	06:40:45.54	09:51:23.1	7.48 ± 0.55	9	0.00	65.0	0.35	-0.09
0640456+092610	06:40:45.62	09:26:10.5	12.23 ± 0.53	2	-99.00	-99.0	0.13	0.01
0640456+094803	06:40:45.69	09:48:03.4	43.53 ± 0.75	2	-99.00	-99.0	-99.00	-0.03
0640458+095946	06:40:45.87	09:59:46.0	21.21 ± 0.04	2	-99.00	-99.0	0.17	-0.11
0640460+091758	06:40:46.01	09:17:58.2	0.27 ± 0.54	6	-99.00	-99.0	0.16	0.08
0640461+094750	06:40:46.10	09:47:50.2	5.60 ± 0.37	2	-99.00	-99.0	0.29	-0.09
0640464+095946	06:40:46.45	09:59:46.4	4.92 ± 1.57	9	-99.00	-99.0	0.11	0.01
0640467+095424	06:40:46.73	09:54:24.7	7.82 ± 0.44	10	-99.00	-99.0	0.19	-0.04
0640470+094607	06:40:47.01	09:46:07.6	9.10 ± 0.03	3	-99.00	-99.0	0.06	-0.05
0640471+091833	06:40:47.13	09:18:33.2	18.04 ± 0.92	7	-99.00	-99.0	0.12	0.03
0640471+092849	06:40:47.18	09:28:49.9	-0.08 ± 0.01	2	-99.00	-99.0	-99.00	0.02
0640471+093240	06:40:47.11	09:32:40.1	3.44 ± 0.42	8	-99.00	-99.0	0.63	0.34
0640471+094207	06:40:47.12	09:42:07.7	3.66 ± 1.14	10	0.52	69.9	0.63	0.26
0640472+095309	06:40:47.21	09:53:09.2	8.59 ± 1.37	3	-99.00	-99.0	0.29	-0.15
0640475+094928	06:40:47.50	09:49:29.0	9.84 ± 0.78	6	0.49	63.0	-18.41	0.25
0640475+100057	06:40:47.57	10:00:57.4	7.42 ± 5.49	2	0.41	71.4	0.23	0.08
0640479+100122	06:40:47.99	10:01:22.5	55.81 ± 0.71	2	-99.00	-99.0	0.18	-0.01
0640486+093252	06:40:48.62	09:32:52.4	0.97 ± 0.13	2	-99.00	-99.0	-99.00	-0.03
0640487+093242	06:40:48.75	09:32:42.5	6.12 ± 1.31	2	0.54	67.8	0.17	0.02
0640488+094325	06:40:48.84	09:43:25.7	12.24 ± 0.81	7	0.59	66.3	1.21	0.53
0640488+094326	06:40:48.80	09:43:26.0	10.88 ± 2.34	2	-99.00	-99.0	-99.00	0.53
0640489+091711	06:40:48.90	09:17:11.6	54.17 ± 1.78	2	-99.00	-99.0	0.09	0.10
0640490+095745	06:40:49.04	09:57:45.1	-24.11 ± 1.07	2	-99.00	-99.0	0.23	-0.02
0640492+095738	06:40:49.21	09:57:38.8	11.12 ± 0.49	8	0.68	68.9	0.26	0.01
0640500+094943	06:40:50.06	09:49:43.0	4.45 ± 0.43	2	-99.00	-99.0	0.08	-0.04
0640500+095227	06:40:50.08	09:52:27.5	3.01 ± 1.04	7	-99.00	-99.0	0.22	0.02
0640501+093725	06:40:50.18	09:37:25.5	-31.10 ± 0.11	6	-99.00	-99.0	0.04	-0.04
0640501+095704	06:40:50.14	09:57:04.0	3.20 ± 0.01	2	0.85	70.9	0.20	0.02
0640503+091954	06:40:50.34	09:19:54.5	-31.85 ± 0.07	5	-99.00	-99.0	-0.04	0.03
0640503+100104	06:40:50.30	10:01:04.3	1.68 ± 1.55	2	0.66	70.6	0.18	-0.01
0640504+094545	06:40:50.49	09:45:45.4	-13.12 ± 0.22	2	-99.00	-99.0	-99.00	0.01
0640504+094850	06:40:50.41	09:48:50.6	70.00 ± 0.01	3	-99.00	-99.0	0.04	-0.01
0640508+095553	06:40:50.86	09:55:53.1	6.24 ± 0.70	2	0.60	67.6	0.10	0.03
0640511+094446	06:40:51.19	09:44:46.1	1.15 ± 0.74	8	-99.00	-99.0	0.93	0.37
0640513+100303	06:40:51.38	10:03:03.0	4.55 ± 1.26	2	-99.00	-99.0	0.17	0.06
0640514+093714	06:40:51.46	09:37:14.5	1.57 ± 0.61	10	0.59	68.0	0.24	-0.05
0640514+094121	06:40:51.42	09:41:21.4	21.33 ± 1.04	2	-99.00	-99.0	-99.00	-0.03

Table 3—Continued

2massID	RA (J2000)	Dec. (J2000)	$\overline{RV}^a$ (km s <sup>-1</sup> )	N Epochs <sup>b</sup>	Lithium EW (Å)	Spectral Type	K - [3.6]	[3.6] - [4.5]
0640515+092844	06:40:51.59	09:28:44.5	4.53 ± 0.16	8	-99.00	-99.0	0.52	0.19
0640515+094324	06:40:51.54	09:43:24.2	7.41 ± 0.44	14	-99.00	-99.0	0.61	0.22
0640522+095231	06:40:52.20	09:52:31.2	4.79 ± 0.57	3	0.74	68.0	0.08	-0.03
0640522+095643	06:40:52.20	09:56:43.3	4.96 ± 1.57	2	-99.00	-99.0	0.23	-0.01
0640525+095058	06:40:52.54	09:50:58.5	3.63 ± 0.23	2	0.55	70.4	0.20	0.06
0640525+095206	06:40:52.55	09:52:06.0	1.83 ± 1.10	2	0.64	69.0	0.30	0.11
0640526+094421	06:40:52.68	09:44:21.0	3.87 ± 0.33	8	0.58	68.0	0.14	-0.06
0640527+092843	06:40:52.73	09:28:43.8	7.01 ± 1.00	3	-99.00	-99.0	-21.47	0.34
0640527+094300	06:40:52.76	09:43:00.4	3.30 ± 1.46	5	-99.00	-99.0	0.47	0.24
0640529+094454	06:40:52.92	09:44:54.4	10.22 ± 0.54	13	0.53	67.7	1.01	0.35
0640536+094704	06:40:53.63	09:47:04.4	1.75 ± 0.90	7	0.46	71.6	0.49	0.27
0640537+095759	06:40:53.71	09:57:59.7	5.62 ± 0.88	3	-99.00	-99.0	0.02	0.08
0640541+095551	06:40:54.20	09:55:52.0	6.05 ± 0.39	10	0.54	67.7	0.04	0.03
0640542+094920	06:40:54.26	09:49:20.4	8.15 ± 0.74	9	-99.00	-99.0	0.83	0.46
0640543+094710	06:40:54.31	09:47:10.7	51.13 ± 0.12	2	-99.00	-99.0	-0.46	-0.16
0640545+100150	06:40:54.55	10:01:50.7	39.12 ± 0.38	3	-99.00	-99.0	0.23	0.03
0640551+095049	06:40:55.18	09:50:49.8	3.85 ± 2.80	3	0.51	68.3	0.14	0.05
0640552+094750	06:40:55.28	09:47:50.4	-23.64 ± 0.24	6	-99.00	-99.0	0.03	-0.08
0640553+093958	06:40:55.32	09:39:58.8	0.71 ± 0.25	2	0.00	72.6	0.99	0.37
0640554+093121	06:40:55.49	09:31:21.8	-14.63 ± 1.14	2	-99.00	-99.0	0.16	-0.07
0640556+093824	06:40:55.62	09:38:24.9	4.02 ± 0.30	3	0.80	71.7	0.25	0.19
0640557+094645	06:40:55.74	09:46:45.7	1.10 ± 0.76	3	0.70	71.8	0.48	0.26
0640563+092113	06:40:56.39	09:21:13.7	20.38 ± 0.00	2	-99.00	-99.0	-99.00	0.07
0640563+093553	06:40:56.40	09:35:53.3	2.84 ± 0.81	5	0.54	66.6	0.93	0.47
0640567+093749	06:40:56.80	09:37:49.0	5.43 ± 0.24	9	-99.00	-99.0	0.32	0.20
0640568+094843	06:40:56.81	09:48:43.5	7.26 ± 1.16	2	0.77	70.8	-99.00	0.32
0640568+094844	06:40:56.83	09:48:44.1	9.08 ± 2.68	2	-99.00	-99.0	-99.00	0.32
0640568+095156	06:40:56.84	09:51:56.6	5.08 ± 0.62	7	0.72	70.5	0.10	0.05
0640569+094840	06:40:56.95	09:48:40.7	8.71 ± 0.03	2	-99.00	-99.0	0.02	-0.02
0640577+093050	06:40:57.77	09:30:50.3	7.85 ± 0.13	2	-99.00	-99.0	0.23	0.03
0640578+095108	06:40:57.84	09:51:08.9	10.82 ± 1.37	7	-99.00	-99.0	0.73	0.31
0640580+091803	06:40:58.00	09:18:03.0	7.36 ± 0.14	7	-99.00	-99.0	-0.06	0.07
0640580+093653	06:40:58.10	09:36:53.4	-0.92 ± 1.30	2	0.53	73.0	0.77	0.34
0640581+095113	06:40:58.10	09:51:13.5	4.46 ± 0.66	3	-99.00	-99.0	0.24	0.05
0640582+095544	06:40:58.20	09:55:44.5	2.45 ± 0.85	2	0.62	70.6	0.20	0.03
0640586+093613	06:40:58.67	09:36:13.3	4.30 ± 1.63	5	0.38	71.8	0.53	0.32
0640586+094554	06:40:58.64	09:45:54.6	26.55 ± 0.43	3	-99.00	-99.0	0.07	0.02
0640588+093057	06:40:58.84	09:30:57.3	5.63 ± 0.63	9	-99.00	-99.0	0.66	0.15
0640588+093918	06:40:58.83	09:39:18.8	4.13 ± 0.45	5	-99.00	-99.0	-99.00	0.11
0640589+092852	06:40:58.92	09:28:52.8	1.63 ± 0.71	7	-99.00	-99.0	0.28	0.17
0640590+094906	06:40:59.04	09:49:06.2	5.27 ± 0.27	2	0.54	69.8	0.16	-0.04
0640593+093333	06:40:59.36	09:33:33.4	7.04 ± 1.64	9	-99.00	-99.0	0.99	0.38
0640594+092951	06:40:59.50	09:29:51.7	2.05 ± 0.49	6	0.47	70.2	-20.42	0.27
0640599+094704	06:40:59.91	09:47:04.4	4.30 ± 0.53	3	0.51	71.4	1.08	0.33

Table 3—Continued

2massID	RA (J2000)	Dec. (J2000)	$\overline{RV}^a$ (km s <sup>-1</sup> )	N Epochs <sup>b</sup>	Lithium EW (Å)	Spectral Type	K - [3.6]	[3.6] - [4.5]
0641000+092850	06:41: 0.00	09:28:50.0	4.48 ± 0.66	10	-99.00	-99.0	0.30	0.02
0641002+093907	06:41: 0.22	09:39:07.0	3.78 ± 2.00	4	0.77	71.5	0.23	0.05
0641002+095849	06:41: 0.25	09:58:49.6	4.58 ± 0.57	11	-99.00	-99.0	0.04	0.02
0641004+095403	06:41: 0.43	09:54:03.5	3.73 ± 2.40	2	-99.00	-99.0	0.16	-0.03
0641006+092151	06:41: 0.70	09:21:51.5	-21.09 ± 0.69	2	-99.00	-99.0	0.27	0.04
0641007+095122	06:41: 0.78	09:51:22.3	4.64 ± 0.26	8	-99.00	-99.0	0.22	-0.01
0641009+093244	06:41: 0.98	09:32:44.4	3.10 ± 0.23	7	-99.00	-99.0	0.94	0.22
0641011+093452	06:41: 1.12	09:34:52.2	6.50 ± 0.42	7	0.47	68.0	-20.71	0.10
0641013+093452	06:41: 1.34	09:34:52.6	5.02 ± 1.01	5	-99.00	-99.0	-21.16	0.26
0641014+093408	06:41: 1.41	09:34:08.1	3.83 ± 0.37	12	-99.00	-99.0	0.17	-0.02
0641015+100036	06:41: 1.53	10:00:36.6	4.38 ± 0.55	2	-99.00	-99.0	0.06	0.19
0641016+092105	06:41: 1.69	09:21:05.6	11.05 ± 0.13	9	-99.00	-99.0	0.11	-0.13
0641017+094242	06:41: 1.72	09:42:43.0	1.64 ± 6.06	2	0.00	69.8	0.88	0.54
0641018+093841	06:41: 1.84	09:38:41.1	5.04 ± 0.49	9	-99.00	-99.0	0.60	0.12
0641020+094535	06:41: 2.05	09:45:35.7	3.69 ± 0.84	2	0.00	69.5	0.22	0.01
0641022+092724	06:41: 2.23	09:27:24.1	4.20 ± 1.48	3	0.64	66.0	0.23	-0.07
0641024+095225	06:41: 2.45	09:52:25.0	8.55 ± 0.34	7	-99.00	-99.0	0.15	0.04
0641025+093455	06:41: 2.54	09:34:55.8	1.75 ± 0.59	2	-99.00	-99.0	-99.00	0.03
0641025+093513	06:41: 2.59	09:35:13.1	3.75 ± 0.40	9	-99.00	-99.0	0.03	-0.04
0641028+091810	06:41: 2.86	09:18:10.1	-17.66 ± 0.61	2	-99.00	-99.0	-99.00	0.03
0641028+100711	06:41: 2.86	10:07:11.9	4.85 ± 1.19	5	-99.00	-99.0	-99.00	-99.00
0641029+094754	06:41: 2.96	09:47:54.3	-7.56 ± 0.51	6	-99.00	-99.0	-0.06	-0.01
0641032+095755	06:41: 3.28	09:57:55.0	2.23 ± 0.23	2	-99.00	-99.0	0.23	0.02
0641033+094044	06:41: 3.38	09:40:44.8	3.65 ± 0.62	11	0.53	69.0	0.14	0.06
0641035+100035	06:41: 3.57	10:00:35.4	4.70 ± 0.25	8	-99.00	-99.0	0.22	0.15
0641037+092739	06:41: 3.74	09:27:39.8	3.33 ± 1.58	2	-99.00	-99.0	0.08	0.09
0641039+095809	06:41: 3.94	09:58:09.5	6.84 ± 1.17	10	-99.00	-99.0	0.19	0.00
0641040+092332	06:41: 4.03	09:23:32.2	7.21 ± 0.27	10	-99.00	-99.0	-0.81	0.25
0641040+093521	06:41: 4.07	09:35:21.1	5.66 ± 1.00	3	0.55	69.0	0.36	0.22
0641040+094908	06:41: 4.04	09:49:08.8	2.39 ± 0.49	10	0.51	66.1	0.33	-0.07
0641041+095202	06:41: 4.18	09:52:02.0	5.16 ± 0.31	2	-99.00	-99.0	0.12	-0.02
0641042+092452	06:41: 4.29	09:24:52.2	1.92 ± 0.43	5	-99.00	-99.0	0.91	0.46
0641043+093547	06:41: 4.32	09:35:47.8	5.90 ± 1.59	2	0.64	71.6	-99.00	0.20
0641043+094822	06:41: 4.34	09:48:22.1	5.31 ± 0.30	11	0.51	62.6	0.23	-0.05
0641044+093643	06:41: 4.44	09:36:43.4	3.95 ± 0.34	2	-99.00	-99.0	0.59	0.29
0641044+095126	06:41: 4.44	09:51:26.1	10.15 ± 0.26	2	-99.00	-99.0	0.10	-0.11
0641044+095318	06:41: 4.47	09:53:18.4	9.81 ± 0.29	10	-99.00	-99.0	0.22	0.15
0641045+092518	06:41: 4.55	09:25:18.3	0.66 ± 1.05	6	0.52	71.6	0.34	-0.01
0641047+093626	06:41: 4.71	09:36:26.7	2.68 ± 0.64	4	-99.00	-99.0	0.04	0.00
0641050+094847	06:41: 5.10	09:48:48.0	8.12 ± 0.26	8	0.68	69.0	0.15	-0.04
0641051+094855	06:41: 5.14	09:48:55.6	1.42 ± 0.59	3	0.62	67.6	0.04	-0.01
0641051+095144	06:41: 5.10	09:51:44.6	6.49 ± 0.47	9	-99.00	-99.0	0.11	0.06
0641051+100018	06:41: 5.18	10:00:19.0	3.97 ± 1.48	5	0.71	72.6	0.33	0.03
0641056+095418	06:41: 5.68	09:54:18.7	5.95 ± 1.28	2	-99.00	-99.0	-99.00	0.01

Table 3—Continued

2massID	RA (J2000)	Dec. (J2000)	$\overline{RV}^a$ (km s <sup>-1</sup> )	N Epochs <sup>b</sup>	Lithium EW (Å)	Spectral Type	K - [3.6]	[3.6] - [4.5]
0641057+093101	06:41: 5.75	09:31:01.3	6.31 ± 0.58	9	-99.00	-99.0	0.56	0.13
0641057+094817	06:41: 5.78	09:48:17.5	9.70 ± 0.57	9	-99.00	-99.0	0.73	0.27
0641058+092255	06:41: 5.88	09:22:55.7	9.75 ± 3.36	3	-99.00	-99.0	1.62	0.47
0641058+095247	06:41: 5.81	09:52:47.9	7.56 ± 0.25	8	-99.00	-99.0	0.07	-0.05
0641059+093551	06:41: 6.00	09:35:51.3	51.92 ± 0.07	2	-99.00	-99.0	0.06	0.05
0641060+093552	06:41: 6.04	09:35:52.0	51.87 ± 0.03	2	-99.00	-99.0	-99.00	0.05
0641062+092503	06:41: 6.23	09:25:03.7	0.14 ± 1.53	7	-99.00	-99.0	0.43	0.29
0641062+093622	06:41: 6.20	09:36:23.0	6.19 ± 0.57	5	-99.00	-99.0	0.41	0.27
0641064+092838	06:41: 6.43	09:28:38.8	4.32 ± 0.51	8	-99.00	-99.0	0.16	0.26
0641067+094727	06:41: 6.73	09:47:27.6	6.53 ± 0.71	5	0.88	71.5	0.59	0.25
0641068+092321	06:41: 6.89	09:23:21.4	1.75 ± 0.02	2	-99.00	-99.0	0.01	-0.03
0641068+092732	06:41: 6.82	09:27:32.3	7.02 ± 0.23	5	-99.00	-99.0	0.70	0.54
0641068+092924	06:41: 6.90	09:29:24.0	4.51 ± 0.64	4	0.88	68.6	0.69	0.38
0641071+091238	06:41: 7.12	09:12:38.3	2.50 ± 0.24	3	-99.00	-99.0	-99.00	0.45
0641071+092729	06:41: 7.16	09:27:29.4	6.27 ± 0.80	5	-99.00	-99.0	0.69	0.45
0641072+095831	06:41: 7.26	09:58:31.2	6.43 ± 1.35	7	-99.00	-99.0	0.09	-0.02
0641073+092554	06:41: 7.34	09:25:55.0	4.62 ± 0.22	7	-99.00	-99.0	-0.09	0.01
0641075+094133	06:41: 7.56	09:41:33.6	-0.40 ± 3.32	2	0.73	71.5	0.34	0.28
0641077+092813	06:41: 7.77	09:28:13.5	2.28 ± 1.33	2	0.00	63.0	0.18	0.04
0641077+094114	06:41: 7.76	09:41:14.9	10.26 ± 0.88	10	-99.00	-99.0	0.12	0.04
0641080+093040	06:41: 8.01	09:30:40.3	8.00 ± 0.38	10	-99.00	-99.0	0.29	0.00
0641081+092322	06:41: 8.12	09:23:22.3	25.96 ± 1.04	2	-99.00	-99.0	0.21	0.11
0641082+093409	06:41: 8.21	09:34:09.5	5.06 ± 1.33	4	-99.00	-99.0	0.52	0.28
0641085+094251	06:41: 8.56	09:42:51.5	5.66 ± 0.45	4	0.57	68.0	0.15	0.03
0641088+094601	06:41: 8.87	09:46:01.1	-6.25 ± 0.72	3	-99.00	-99.0	-0.01	-0.02
0641088+095301	06:41: 8.86	09:53:01.1	4.21 ± 0.63	5	0.35	69.7	0.40	0.35
0641089+093346	06:41: 8.96	09:33:46.0	3.60 ± 1.09	11	0.45	71.8	0.43	0.29
0641089+094114	06:41: 8.92	09:41:14.8	4.83 ± 0.27	2	0.84	65.0	0.10	0.07
0641089+095647	06:41: 8.93	09:56:47.6	7.18 ± 3.25	2	-99.00	-99.0	0.33	0.00
0641090+093009	06:41: 9.09	09:30:09.1	5.47 ± 0.50	5	-99.00	-99.0	1.30	0.45
0641091+095301	06:41: 9.20	09:53:01.5	4.10 ± 0.99	9	-99.00	-99.0	0.14	0.09
0641091+095302	06:41: 9.19	09:53:02.1	4.18 ± 0.34	2	-99.00	-99.0	-99.00	0.09
0641095+093525	06:41: 9.51	09:35:25.5	7.85 ± 2.29	8	-99.00	-99.0	0.14	-0.02
0641099+093020	06:41: 9.91	09:30:20.7	4.51 ± 1.96	2	-99.00	-99.0	-21.91	0.33
0641101+093128	06:41:10.14	09:31:28.5	3.93 ± 1.29	4	0.82	71.4	0.24	0.06
0641103+092149	06:41:10.31	09:21:49.5	1.21 ± 0.54	2	-99.00	-99.0	0.15	0.09
0641107+094641	06:41:10.79	09:46:41.2	1.77 ± 1.18	2	-99.00	-99.0	0.31	0.08
0641107+095742	06:41:10.70	09:57:42.5	8.58 ± 0.28	8	-99.00	-99.0	0.68	0.30
0641109+093555	06:41:11.00	09:35:55.7	5.12 ± 0.90	4	0.26	68.5	1.10	0.49
0641115+100223	06:41:11.59	10:02:23.6	5.97 ± 0.64	10	-99.00	-99.0	0.15	0.02
0641118+092332	06:41:11.82	09:23:32.6	0.29 ± 1.77	2	-99.00	-99.0	0.17	0.10
0641127+095944	06:41:12.71	09:59:44.6	-21.13 ± 0.46	2	-99.00	-99.0	0.31	-0.02
0641128+092614	06:41:12.87	09:26:14.9	4.62 ± 0.65	10	-99.00	-99.0	0.95	0.59
0641128+094600	06:41:12.89	09:46:00.8	0.53 ± 0.48	2	-99.00	-99.0	0.25	0.07



Table 3—Continued

2massID	RA (J2000)	Dec. (J2000)	$\overline{RV}^a$ (km s <sup>-1</sup> )	N Epochs <sup>b</sup>	Lithium EW (Å)	Spectral Type	K - [3.6]	[3.6] - [4.5]
0641128+095243	06:41:12.82	09:52:43.4	6.37 ± 0.47	9	-99.00	-99.0	0.17	-0.06
0641129+090525	06:41:12.92	09:05:25.7	1.64 ± 0.69	2	-99.00	-99.0	-99.00	-99.00
0641129+093532	06:41:12.96	09:35:32.3	4.78 ± 0.52	2	0.73	69.9	0.14	-0.06
0641130+092740	06:41:13.00	09:27:40.0	7.53 ± 0.10	2	-99.00	-99.0	-21.05	-0.01
0641132+095508	06:41:13.22	09:55:08.7	-0.77 ± 0.93	2	-99.00	-99.0	0.25	0.06
0641133+092807	06:41:13.33	09:28:07.5	4.42 ± 0.47	2	0.61	67.4	0.09	0.01
0641133+095154	06:41:13.30	09:51:54.4	5.81 ± 0.14	2	0.73	69.2	0.14	0.05
0641138+094542	06:41:13.87	09:45:42.5	-25.71 ± 0.14	6	-99.00	-99.0	0.06	0.01
0641144+093321	06:41:14.47	09:33:21.4	5.45 ± 0.33	6	-99.00	-99.0	0.18	0.03
0641144+093714	06:41:14.48	09:37:14.3	3.34 ± 0.50	10	0.59	68.0	0.13	0.05
0641147+093413	06:41:14.75	09:34:13.5	3.86 ± 0.28	7	0.51	69.1	1.45	0.46
0641148+092555	06:41:14.86	09:25:55.1	6.25 ± 2.59	3	-99.00	-99.0	-20.26	0.50
0641148+093235	06:41:14.85	09:32:35.8	8.43 ± 1.66	5	-99.00	-99.0	0.53	-0.03
0641152+093757	06:41:15.21	09:37:57.6	4.29 ± 0.86	3	-99.00	-99.0	0.54	0.32
0641154+094012	06:41:15.47	09:40:12.6	-44.18 ± 0.14	5	-99.00	-99.0	-0.05	0.00
0641154+094639	06:41:15.43	09:46:39.6	2.72 ± 0.83	7	-99.00	-99.0	0.12	-0.06
0641157+092616	06:41:15.75	09:26:16.8	2.98 ± 0.64	5	-99.00	-99.0	0.13	-0.04
0641157+093818	06:41:15.72	09:38:18.2	-10.61 ± 0.08	6	-99.00	-99.0	0.00	0.04
0641159+092609	06:41:15.99	09:26:09.5	4.10 ± 1.63	4	-99.00	-99.0	0.50	0.68
0641165+095213	06:41:16.52	09:52:13.2	40.53 ± 0.24	2	-99.00	-99.0	-0.01	0.00
0641167+092730	06:41:16.78	09:27:30.2	0.79 ± 0.52	8	-99.00	-99.0	0.42	0.28
0641170+093252	06:41:17.06	09:32:52.3	3.88 ± 1.96	2	-99.00	-99.0	0.25	0.00
0641170+095240	06:41:17.10	09:52:40.5	9.09 ± 0.69	9	-99.00	-99.0	0.23	-0.03
0641172+095432	06:41:17.25	09:54:32.4	4.41 ± 0.02	2	0.38	66.2	1.06	0.47
0641177+092926	06:41:17.71	09:29:26.2	8.56 ± 0.84	7	-99.00	-99.0	0.34	-0.01
0641179+092901	06:41:17.92	09:29:01.1	10.25 ± 1.13	2	-99.00	-99.0	0.69	0.51
0641180+093825	06:41:18.08	09:38:25.4	3.39 ± 3.56	2	0.48	72.6	0.35	0.04
0641182+093353	06:41:18.27	09:33:53.6	5.01 ± 0.32	9	-99.00	-99.0	0.16	0.05
0641183+093941	06:41:18.37	09:39:41.1	6.02 ± 0.86	8	0.30	68.4	0.31	0.10
0641183+094406	06:41:18.31	09:44:06.8	5.51 ± 0.66	2	0.56	69.5	0.56	0.33
0641183+094407	06:41:18.30	09:44:07.1	6.05 ± 0.65	2	-99.00	-99.0	-99.00	0.33
0641188+093944	06:41:18.90	09:39:44.0	12.99 ± 0.36	8	-99.00	-99.0	0.14	-0.10
0641189+092715	06:41:18.93	09:27:15.8	1.04 ± 0.03	2	0.66	77.2	0.21	0.10
0641189+093554	06:41:18.90	09:35:54.2	2.66 ± 0.95	3	0.00	71.5	0.43	0.23
0641194+093028	06:41:19.45	09:30:28.6	32.29 ± 0.12	5	-99.00	-99.0	-0.01	-0.04
0641198+092704	06:41:19.85	09:27:04.8	1.45 ± 0.62	2	-99.00	-99.0	0.18	0.08
0641205+094535	06:41:20.54	09:45:35.5	2.06 ± 0.30	8	0.49	67.1	0.17	0.03
0641205+094730	06:41:20.54	09:47:30.0	1.86 ± 0.81	2	0.56	67.0	0.18	0.04
0641207+092845	06:41:20.71	09:28:45.3	2.09 ± 2.70	2	1.14	71.3	0.53	0.31
0641207+094315	06:41:20.73	09:43:15.6	74.73 ± 0.31	2	-99.00	-99.0	0.43	0.02
0641214+095835	06:41:21.42	09:58:35.5	-14.14 ± 0.40	2	-99.00	-99.0	0.07	-0.08
0641217+094530	06:41:21.79	09:45:31.0	4.76 ± 0.19	9	0.41	65.8	-0.03	0.01
0641220+094312	06:41:22.02	09:43:12.7	3.54 ± 0.39	9	0.56	66.0	0.15	0.00
0641220+095112	06:41:22.03	09:51:12.7	3.48 ± 0.38	8	0.49	67.0	0.16	-0.07

Table 3—Continued

2massID	RA (J2000)	Dec. (J2000)	$\overline{RV}^a$ (km s <sup>-1</sup> )	N Epochs <sup>b</sup>	Lithium EW (Å)	Spectral Type	K - [3.6]	[3.6] - [4.5]
0641225+092912	06:41:22.54	09:29:12.9	-10.77 ± 0.38	2	-99.00	-99.0	0.06	-0.05
0641231+093733	06:41:23.14	09:37:33.9	4.87 ± 1.51	7	0.57	70.6	0.79	0.32
0641232+093036	06:41:23.20	09:30:36.4	-0.19 ± 1.57	2	0.76	69.5	0.10	0.13
0641234+094558	06:41:23.46	09:45:58.6	1.84 ± 0.01	2	0.43	68.0	-99.00	0.00
0641236+094716	06:41:23.63	09:47:16.4	1.23 ± 1.29	2	-99.00	-99.0	-22.14	0.04
0641237+093356	06:41:23.79	09:33:56.5	-6.60 ± 1.63	5	-99.00	-99.0	0.05	-0.01
0641242+093154	06:41:24.25	09:31:54.2	6.35 ± 0.19	2	-99.00	-99.0	0.11	0.00
0641243+092139	06:41:24.39	09:21:39.0	-21.16 ± 0.07	2	-99.00	-99.0	-99.00	0.05
0641245+093735	06:41:24.54	09:37:35.5	3.93 ± 3.27	2	-99.00	-99.0	0.25	0.04
0641250+094242	06:41:25.02	09:42:42.1	2.02 ± 0.49	7	0.56	70.4	0.10	0.00
0641256+094403	06:41:25.63	09:44:03.3	3.55 ± 0.61	2	1.09	70.8	-99.00	0.28
0641262+093448	06:41:26.28	09:34:48.3	21.79 ± 0.31	5	-99.00	-99.0	0.06	-0.05
0641262+094722	06:41:26.22	09:47:22.5	38.80 ± 0.37	2	-99.00	-99.0	0.18	0.08
0641264+094405	06:41:26.49	09:44:05.8	4.13 ± 0.03	2	0.23	65.6	-99.00	0.09
0641266+092354	06:41:26.67	09:23:54.7	25.70 ± 0.99	5	-99.00	-99.0	0.00	0.00
0641270+093013	06:41:27.00	09:30:13.1	4.96 ± 0.62	6	0.20	69.9	0.19	0.04
0641275+093155	06:41:27.56	09:31:55.8	23.72 ± 0.32	3	-99.00	-99.0	0.08	-0.10
0641282+093459	06:41:28.30	09:34:60.0	160.40 ± 0.11	4	-99.00	-99.0	0.08	-0.03
0641287+092710	06:41:28.74	09:27:10.8	4.24 ± 3.00	2	-99.00	-99.0	0.16	0.00
0641288+100914	06:41:28.85	10:09:14.5	7.80 ± 0.08	4	-99.00	-99.0	-99.00	-99.00
0641291+093936	06:41:29.19	09:39:36.0	4.88 ± 0.59	3	-99.00	-99.0	0.08	-0.06
0641294+093918	06:41:29.45	09:39:18.2	4.15 ± 0.37	2	0.65	68.0	-99.00	0.02
0641307+094259	06:41:30.75	09:42:59.6	25.99 ± 0.21	3	-99.00	-99.0	0.17	0.03
0641309+092020	06:41:30.97	09:20:20.0	-0.15 ± 1.76	5	-99.00	-99.0	0.27	-0.07
0641311+092658	06:41:31.12	09:26:58.2	2.49 ± 0.73	9	-99.00	-99.0	0.89	0.33
0641319+095514	06:41:31.95	09:55:14.7	115.35 ± 0.17	2	-99.00	-99.0	-99.00	-0.02
0641325+093807	06:41:32.50	09:38:07.4	2.44 ± 0.41	9	-99.00	-99.0	0.07	0.03
0641325+094536	06:41:32.58	09:45:36.4	36.42 ± 1.36	2	-99.00	-99.0	-99.00	-0.08
0641327+095324	06:41:32.70	09:53:24.1	-12.88 ± 1.60	2	-99.00	-99.0	0.15	0.05
0641332+094146	06:41:33.28	09:41:46.1	73.99 ± 0.18	2	-99.00	-99.0	0.20	-0.06
0641335+094321	06:41:33.59	09:43:21.4	20.02 ± 0.13	2	-99.00	-99.0	0.19	0.07
0641340+095848	06:41:34.00	09:58:48.6	11.02 ± 0.10	2	-99.00	-99.0	-99.00	0.00
0641342+093442	06:41:34.26	09:34:42.4	49.06 ± 0.20	5	-99.00	-99.0	0.26	0.06
0641343+092553	06:41:34.34	09:25:53.4	-0.00 ± 4.51	2	-99.00	-99.0	0.22	0.04
0641343+100225	06:41:34.38	10:02:25.1	-0.69 ± 0.31	2	-99.00	-99.0	-99.00	-0.02
0641345+093632	06:41:34.56	09:36:32.5	4.48 ± 0.94	9	0.68	68.6	0.27	-0.02
0641354+091850	06:41:35.48	09:18:50.3	-1.28 ± 0.88	2	-99.00	-99.0	0.32	0.14
0641354+094919	06:41:35.42	09:49:19.2	-12.74 ± 0.33	2	-99.00	-99.0	0.30	0.03
0641357+100415	06:41:35.74	10:04:15.8	3.50 ± 1.49	4	-99.00	-99.0	-99.00	0.04
0641358+094042	06:41:35.89	09:40:42.0	6.46 ± 0.51	2	0.76	70.8	0.02	0.08
0641360+095433	06:41:36.00	09:54:33.1	27.80 ± 0.98	2	-99.00	-99.0	-99.00	0.00
0641362+093920	06:41:36.24	09:39:20.4	1.22 ± 0.45	11	0.60	67.6	0.10	0.07
0641367+095337	06:41:36.71	09:53:38.0	38.72 ± 0.87	5	-99.00	-99.0	0.15	0.08
0641367+095819	06:41:36.73	09:58:19.8	57.91 ± 0.22	2	-99.00	-99.0	-99.00	-0.03

Table 3—Continued

2massID	RA (J2000)	Dec. (J2000)	$\overline{RV}^a$ (km s <sup>-1</sup> )	N Epochs <sup>b</sup>	Lithium EW (Å)	Spectral Type	K - [3.6]	[3.6] - [4.5]
0641372+094506	06:41:37.29	09:45:06.7	1.93 ± 0.26	5	-99.00	-99.0	0.43	0.16
0641373+095837	06:41:37.33	09:58:37.6	-19.99 ± 0.16	3	-99.00	-99.0	-0.05	-0.03
0641375+094040	06:41:37.54	09:40:40.8	-23.57 ± 0.56	3	-99.00	-99.0	0.11	0.03
0641377+094533	06:41:37.78	09:45:33.3	9.84 ± 0.17	2	-99.00	-99.0	0.22	-0.03
0641381+095746	06:41:38.16	09:57:46.7	73.32 ± 0.22	6	-99.00	-99.0	0.17	0.00
0641382+093213	06:41:38.28	09:32:13.3	68.41 ± 0.19	4	-99.00	-99.0	0.20	0.01
0641387+093211	06:41:38.77	09:32:11.8	1.18 ± 0.26	9	-99.00	-99.0	0.86	0.28
0641389+100935	06:41:38.91	10:09:35.5	5.88 ± 0.11	6	-99.00	-99.0	-99.00	-99.00
0641390+092938	06:41:39.05	09:29:38.1	23.01 ± 0.67	3	-99.00	-99.0	0.23	0.07
0641394+100002	06:41:39.43	10:00:02.1	48.81 ± 0.22	2	-99.00	-99.0	0.02	-0.08
0641396+094141	06:41:39.63	09:41:41.0	26.49 ± 0.20	2	-99.00	-99.0	0.15	0.05
0641397+094027	06:41:39.75	09:40:27.9	3.96 ± 0.50	2	-99.00	-99.0	0.71	0.25
0641406+093558	06:41:40.67	09:35:58.2	62.48 ± 0.23	5	-99.00	-99.0	0.07	0.01
0641411+093354	06:41:41.15	09:33:54.6	10.51 ± 0.09	3	-99.00	-99.0	0.17	-0.02
0641414+094053	06:41:41.40	09:40:53.6	42.53 ± 0.37	5	-99.00	-99.0	0.16	-0.03
0641415+094613	06:41:41.59	09:46:13.5	73.69 ± 0.06	2	-99.00	-99.0	-99.00	-0.05
0641420+094736	06:41:42.06	09:47:36.1	4.19 ± 0.25	7	-99.00	-99.0	-0.02	0.02
0641424+095031	06:41:42.43	09:50:31.4	90.15 ± 0.00	2	-99.00	-99.0	-99.00	-0.05
0641427+094245	06:41:42.73	09:42:45.9	0.94 ± 0.22	2	0.82	72.4	-99.00	0.06
0641427+094256	06:41:42.74	09:42:56.6	0.57 ± 0.63	6	-99.00	-99.0	0.12	0.07
0641428+092508	06:41:42.88	09:25:08.4	3.93 ± 0.57	9	-99.00	-99.0	0.55	0.23
0641429+092327	06:41:42.92	09:23:27.9	1.35 ± 0.53	7	-99.00	-99.0	0.27	0.07
0641434+095652	06:41:43.44	09:56:52.8	25.50 ± 0.16	6	-99.00	-99.0	0.14	0.00
0641438+094104	06:41:43.87	09:41:04.4	47.13 ± 0.09	4	-99.00	-99.0	0.07	-0.08
0641439+091757	06:41:43.99	09:17:57.1	24.86 ± 1.55	2	-99.00	-99.0	0.27	0.10
0641442+094129	06:41:44.23	09:41:29.7	52.60 ± 0.28	4	-99.00	-99.0	0.13	0.01
0641443+093035	06:41:44.38	09:30:35.0	119.64 ± 0.65	2	-99.00	-99.0	0.23	-0.03
0641444+093935	06:41:44.46	09:39:35.9	-13.81 ± 0.64	2	-99.00	-99.0	0.13	-0.03
0641449+094440	06:41:44.94	09:44:40.4	3.08 ± 0.11	9	0.53	66.6	0.09	-0.02
0641450+095611	06:41:45.00	09:56:11.3	24.24 ± 0.09	4	-99.00	-99.0	0.15	-0.01
0641456+093931	06:41:45.60	09:39:31.2	1.32 ± 3.31	2	-99.00	-99.0	0.20	0.08
0641457+092642	06:41:45.76	09:26:42.8	6.08 ± 3.45	5	-99.00	-99.0	0.21	0.09
0641459+093302	06:41:45.91	09:33:02.5	25.76 ± 0.14	3	-99.00	-99.0	0.19	-0.04
0641464+094306	06:41:46.44	09:43:06.8	2.24 ± 0.21	7	0.51	68.0	0.07	0.01
0641466+092400	06:41:46.68	09:24:00.1	3.52 ± 0.94	2	-99.00	-99.0	-99.00	0.00
0641471+093804	06:41:47.11	09:38:04.7	2.27 ± 0.89	2	0.70	65.0	0.13	-0.06
0641472+093515	06:41:47.22	09:35:15.3	17.06 ± 1.74	2	-99.00	-99.0	0.20	0.04
0641474+094200	06:41:47.42	09:42:00.3	3.46 ± 0.40	6	0.69	69.1	0.14	0.05
0641474+094550	06:41:47.42	09:45:50.2	-21.65 ± 0.02	2	-99.00	-99.0	0.04	0.04
0641480+094243	06:41:48.06	09:42:43.3	1.92 ± 0.97	8	-99.00	-99.0	0.08	-0.03
0641481+094253	06:41:48.19	09:42:53.3	-13.55 ± 0.10	5	-99.00	-99.0	0.02	0.01
0641488+094313	06:41:48.87	09:43:13.4	10.62 ± 0.40	4	-99.00	-99.0	0.26	-0.14
0641490+094106	06:41:49.02	09:41:06.1	1.56 ± 0.31	8	-99.00	-99.0	0.12	0.01
0641504+093927	06:41:50.41	09:39:27.1	20.20 ± 0.28	2	-99.00	-99.0	0.19	-0.07

Table 3—Continued

2massID	RA (J2000)	Dec. (J2000)	$\overline{RV}^a$ (km s <sup>-1</sup> )	N Epochs <sup>b</sup>	Lithium EW (Å)	Spectral Type	K - [3.6]	[3.6] - [4.5]
0641504+094601	06:41:50.46	09:46:01.7	35.68 ± 0.24	5	-99.00	-99.0	0.23	-0.10
0641508+094725	06:41:50.87	09:47:25.8	-10.26 ± 0.21	4	-99.00	-99.0	0.23	-0.12
0641510+094200	06:41:51.04	09:42:00.4	1.64 ± 3.44	2	0.00	72.1	-99.00	0.16
0641514+094409	06:41:51.48	09:44:09.7	0.99 ± 0.89	7	-99.00	-99.0	0.25	0.03
0641514+095342	06:41:51.46	09:53:42.6	4.57 ± 0.43	9	-99.00	-99.0	0.04	0.01
0641518+093256	06:41:51.84	09:32:56.6	76.39 ± 0.10	2	-99.00	-99.0	-99.00	-0.01
0641521+094622	06:41:52.19	09:46:22.1	-7.16 ± 0.10	2	-99.00	-99.0	0.18	0.04
0641530+094915	06:41:53.06	09:49:15.9	25.69 ± 0.25	2	-99.00	-99.0	0.18	0.10
0641530+100002	06:41:53.06	10:00:02.3	-15.72 ± 0.53	3	-99.00	-99.0	0.27	0.11
0641531+095047	06:41:53.16	09:50:47.4	5.54 ± 0.17	5	-99.00	-99.0	0.36	0.25
0641536+094203	06:41:53.69	09:42:03.3	-10.51 ± 0.09	5	-99.00	-99.0	0.03	-0.09
0641536+094615	06:41:53.61	09:46:15.0	2.48 ± 0.56	2	-99.00	-99.0	0.24	-0.04
0641544+092915	06:41:54.48	09:29:16.0	1.10 ± 0.10	5	-99.00	-99.0	0.15	-0.01
0641546+094127	06:41:54.69	09:41:27.2	-0.71 ± 0.03	2	-99.00	-99.0	0.16	-0.05
0641548+092528	06:41:54.84	09:25:28.9	30.17 ± 0.22	4	-99.00	-99.0	0.26	-0.09
0641549+094252	06:41:54.93	09:42:52.7	-0.94 ± 2.16	4	0.40	70.0	0.11	0.10
0641557+093958	06:41:55.79	09:39:58.0	0.33 ± 0.55	2	0.24	69.7	0.10	0.03
0641563+095005	06:41:56.36	09:50:05.9	0.89 ± 0.07	6	-99.00	-99.0	0.01	-0.04
0641567+093407	06:41:56.72	09:34:07.8	13.43 ± 0.46	2	-99.00	-99.0	0.14	-0.05
0641571+095741	06:41:57.15	09:57:41.5	27.92 ± 0.07	4	-99.00	-99.0	0.24	-0.11
0641580+094306	06:41:58.04	09:43:06.2	6.56 ± 0.66	8	0.57	66.6	0.12	0.01
0641580+095054	06:41:58.03	09:50:54.2	40.04 ± 0.16	2	-99.00	-99.0	-99.00	-0.09
0641585+093936	06:41:58.56	09:39:36.8	-4.22 ± 0.66	2	0.00	65.4	-99.00	0.03
0641590+092621	06:41:59.01	09:26:21.4	32.16 ± 0.08	5	-99.00	-99.0	0.11	0.03
0642011+100026	06:42: 1.11	10:00:26.2	87.48 ± 0.03	3	-99.00	-99.0	0.11	20.15
0642025+093652	06:42: 2.56	09:36:52.5	2.39 ± 0.51	9	0.93	66.3	-0.13	0.06
0642026+095827	06:42: 2.68	09:58:27.9	9.56 ± 0.22	5	-99.00	-99.0	0.10	21.55
0642029+092729	06:42: 2.98	09:27:29.2	22.14 ± 0.47	5	-99.00	-99.0	0.20	-0.04
0642030+093413	06:42: 3.03	09:34:13.9	21.58 ± 0.14	2	-99.00	-99.0	0.16	19.84
0642033+093713	06:42: 3.37	09:37:13.0	-9.39 ± 1.00	2	-99.00	-99.0	-99.00	-99.00
0642037+094122	06:42: 3.71	09:41:22.1	38.29 ± 0.20	2	-99.00	-99.0	0.26	-0.06
0642037+094959	06:42: 3.79	09:49:59.2	23.82 ± 1.03	2	-99.00	-99.0	0.15	0.05
0642042+093728	06:42: 4.20	09:37:28.6	45.05 ± 2.24	2	-99.00	-99.0	-99.00	-99.00
0642044+094238	06:42: 4.49	09:42:38.2	40.80 ± 0.11	2	-99.00	-99.0	0.09	-0.15
0642056+094436	06:42: 5.60	09:44:36.5	-88.87 ± 0.35	4	-99.00	-99.0	21.87	-21.53
0642071+095344	06:42: 7.16	09:53:44.5	9.72 ± 0.33	4	-99.00	-99.0	0.13	-0.03
0642071+100013	06:42: 7.12	10:00:13.9	59.79 ± 0.14	4	-99.00	-99.0	0.23	20.46
0642073+094947	06:42: 7.36	09:49:47.1	15.93 ± 0.27	4	-99.00	-99.0	0.27	-0.12
0642078+094652	06:42: 7.86	09:46:52.4	-21.21 ± 0.13	5	-99.00	-99.0	-99.00	-99.00
0642084+093321	06:42: 8.43	09:33:21.8	22.28 ± 0.23	2	-99.00	-99.0	-99.00	-99.00
0642087+094121	06:42: 8.70	09:41:21.2	2.34 ± 0.66	9	-99.00	-99.0	-99.00	-99.00
0642089+094208	06:42: 8.93	09:42:08.6	3.92 ± 0.55	2	-99.00	-99.0	-99.00	-99.00
0642091+094804	06:42: 9.15	09:48:04.9	11.55 ± 0.19	10	-99.00	-99.0	-99.00	-99.00
0642091+095902	06:42: 9.11	09:59:02.8	14.53 ± 0.21	9	-99.00	-99.0	0.19	19.48

Table 3—Continued

2massID	RA (J2000)	Dec. (J2000)	$\overline{RV}^a$ (km s <sup>-1</sup> )	N Epochs <sup>b</sup>	Lithium EW (Å)	Spectral Type	K - [3.6]	[3.6] - [4.5]
0642091+095945	06:42: 9.12	09:59:45.5	45.84 ± 0.20	3	-99.00	-99.0	0.14	21.22
0642092+094403	06:42: 9.24	09:44:03.4	2.45 ± 0.44	9	-99.00	-99.0	-99.00	-99.00
0642094+093205	06:42: 9.48	09:32:05.5	-95.64 ± 0.14	5	-99.00	-99.0	-99.00	-99.00
0642098+094522	06:42: 9.89	09:45:22.1	44.22 ± 0.22	5	-99.00	-99.0	-99.00	-99.00
0642101+094024	06:42:10.10	09:40:25.0	-18.38 ± 0.22	4	-99.00	-99.0	-99.00	-99.00
0642102+093604	06:42:10.22	09:36:04.5	30.65 ± 0.10	5	-99.00	-99.0	-99.00	-99.00
0642103+095914	06:42:10.33	09:59:14.6	55.69 ± 0.14	2	-99.00	-99.0	0.22	21.14
0642107+095559	06:42:10.77	09:55:59.6	68.44 ± 1.89	2	-99.00	-99.0	-99.00	-99.00
0642113+092903	06:42:11.37	09:29:03.3	-15.71 ± 0.21	5	-99.00	-99.0	-99.00	-99.00
0642113+092904	06:42:11.35	09:29:04.4	-16.94 ± 1.34	2	-99.00	-99.0	-99.00	-99.00
0642113+094345	06:42:11.38	09:43:45.6	-0.21 ± 1.84	2	-99.00	-99.0	-99.00	-99.00
0642114+093423	06:42:11.43	09:34:23.9	23.54 ± 0.05	2	-99.00	-99.0	-99.00	-99.00
0642125+095907	06:42:12.57	09:59:07.1	8.96 ± 1.02	6	-99.00	-99.0	-99.00	-99.00
0642126+093131	06:42:12.67	09:31:31.6	59.96 ± 0.32	5	-99.00	-99.0	-99.00	-99.00
0642127+093009	06:42:12.74	09:30:09.1	66.97 ± 0.20	7	-99.00	-99.0	-99.00	-99.00
0642131+094603	06:42:13.13	09:46:03.5	14.35 ± 0.27	9	-99.00	-99.0	-99.00	-99.00
0642139+095012	06:42:13.95	09:50:12.6	-15.45 ± 0.08	2	-99.00	-99.0	-99.00	-99.00
0642141+094308	06:42:14.15	09:43:08.9	-34.91 ± 0.10	5	-99.00	-99.0	-99.00	-99.00
0642154+092637	06:42:15.46	09:26:37.2	6.52 ± 0.36	2	-99.00	-99.0	-99.00	-99.00
0642157+094033	06:42:15.77	09:40:33.1	-64.86 ± 0.15	5	-99.00	-99.0	-99.00	-99.00
0642166+093400	06:42:16.67	09:34:00.4	-7.14 ± 0.05	2	-99.00	-99.0	-99.00	-99.00
0642167+093652	06:42:16.75	09:36:52.9	16.26 ± 1.74	2	-99.00	-99.0	-99.00	-99.00
0642169+093351	06:42:16.99	09:33:51.3	76.17 ± 0.28	4	-99.00	-99.0	-99.00	-99.00
0642169+094725	06:42:16.91	09:47:25.2	13.54 ± 0.12	3	-99.00	-99.0	-99.00	-99.00
0642177+094052	06:42:17.79	09:40:52.0	78.21 ± 0.21	2	-99.00	-99.0	-99.00	-99.00
0642198+093102	06:42:19.88	09:31:02.0	-7.19 ± 0.12	2	-99.00	-99.0	-99.00	-99.00
0642200+093850	06:42:20.07	09:38:50.2	82.75 ± 0.08	5	-99.00	-99.0	-99.00	-99.00
0642202+093704	06:42:20.27	09:37:04.5	7.76 ± 1.43	6	-99.00	-99.0	-99.00	-99.00
0642227+094612	06:42:22.77	09:46:12.4	21.89 ± 0.48	2	-99.00	-99.0	-99.00	-99.00
0642245+093126	06:42:24.52	09:31:26.2	8.97 ± 0.47	2	-99.00	-99.0	-99.00	-99.00
0642256+094115	06:42:25.69	09:41:15.6	19.51 ± 0.20	2	-99.00	-99.0	-99.00	-99.00
0642257+094151	06:42:25.77	09:41:51.5	36.88 ± 0.07	2	-99.00	-99.0	-99.00	-99.00
0642265+094030	06:42:26.57	09:40:30.4	43.92 ± 0.11	2	-99.00	-99.0	-99.00	-99.00
0642266+093750	06:42:26.69	09:37:50.4	46.67 ± 0.09	2	-99.00	-99.0	-99.00	-99.00
0642272+093940	06:42:27.20	09:39:40.6	-25.20 ± 0.24	2	-99.00	-99.0	-99.00	-99.00

Note. — Abridged table of target IDs, positions, average radial velocities, Lithium 6707 Å Equivalent Widths, Spectral Types, and near infrared colors. Entries with -99 signify that these data are unavailable for a given target.

<sup>a</sup>Velocities from Fűrész et al. (2006) are included in average. For a measurement to be included in the average R must be > 6.0; R is defined in Equation 1.

<sup>b</sup>Number of observations with R > 6.0.